autoantigen directly affecting its interaction with autoantibodies.

REFERENCES

1. Hughes GR. The antiphospholipid syndrome: ten years on. Lancet 1993;342:341–4.
2. Hughes GR, Harris EN, Gharavi AE. The anticardiolipin syndrome. J Rheumatol 1986;13:486–9.
3. Harris EN, Gharavi AE, Hughes GR. Anti-phospholipid antibodies. Clin Rheum Dis 1985;11:591–609.
4. Galli M, Comfurius P, Maassen C, Hemker HC, de Baets MH, van Breda-Vriesman PJ, et al. Anticardiolipin antibodies (ACA) directed not to cardiolipin but to a plasma protein cofactor. Lancet 1990;335:1544–7.
5. McNeil HP, Simpson RJ, Chesterman CN, Krilis SA. Anti-phospholipid antibodies are directed against a complex antigen that includes a lipid-binding inhibitor of coagulation: β_2-glycoprotein I (apolipoprotein H). Proc Natl Acad Sci U S A 1990;87:4120–4.
6. Matsuura E, Igarashi Y, Fujimoto M, Ichikawa K, Koike T. Anticardiolipin cofactor(s) and differential diagnosis of autoimmune disease. Lancet 1990;336:177–8.
7. Matsuura E, Igarashi Y, Yasuda T, Triplett DA, Koike T. Anticardiolipin antibodies recognize β_2-glycoprotein I structure altered by interacting with an oxygen modified solid phase surface. J Exp Med 1994;179:457–62.
8. Roubey RA, Eisenberg RA, Harper MF, Winfield JB. "Anticardiolipin" autoantibodies recognize β_2-glycoprotein I in the absence of phospholipid: importance of Ag density and bivalent binding. J Immunol 1995;154:954–60.
9. Schwarzenbacher R, Zeth K, Diederichs K, Gries A, Kostner GM, Laggner P, et al. Crystal structure of human β_2-glycoprotein I: implications for phospholipid binding and the antiphospholipid syndrome. EMBO J 1999;18:6228–39.
10. Sanghera DK, Kristensen T, Hamman RF, Kamboh MI. Molecular basis of the apolipoprotein H (β_2-glycoprotein I) protein polymorphism. Hum Genet 1997;100:57–62.
11. Yasuda S, Tsutsumi A, Chiba H, Yanai H, Miyoshi Y, Takeuchi R, et al. β_2-glycoprotein I deficiency: prevalence, genetic background and effects on plasma lipoprotein metabolism and hemostasis. Atherosclerosis 2000;152:337–46.
12. Igarashi M, Matsuura E, Igarashi Y, Nagae H, Ichikawa K, Triplett DA, et al. Human β_2-glycoprotein I as an anticardiolipin cofactor determined using mutants expressed by a baculovirus system. Blood 1996;87:3262–70.
13. Iverson GM, Victoria EJ, Marquis DM. Anti-β_2 glycoprotein I (β_2GPI) autoantibodies recognize an epitope on the first domain of β_2GPI. Proc Natl Acad Sci U S A 1998;95:15542–6.
14. Wang MX, Kandiah DA, Ichikawa K, Khamashta M, Hughes G, Koike T, et al. Epitope specificity of monoclonal anti-β_2-glycoprotein I antibodies derived from patients with the antiphospholipid syndrome. J Immunol 1995;155:1629–36.
15. Atsumi T, Tsutsumi A, Amengual O, Khamashta MA, Hughes GR, Miyoshi Y, et al. Correlation between β_2-glycoprotein I valine/leucine^{247} polymorphism and anti-β_2-glycoprotein I antibodies in patients with primary antiphospholipid syndrome. Rheumatology (Oxford) 1999;38:721–3.
16. Matsuura E, Igarashi Y, Fujimoto M, Ichikawa K, Suzuki T, Sumida T, et al. Heterogeneity of anticardiolipin antibodies defined by the anticardiolipin cofactor. J Immunol 1992;148:3885–91.
17. Atsumi T, Ieko M, Bertolaccini ML, Ichikawa K, Tsutsumi A, Matsuura E, et al. Association of autoantibodies against the phosphatidylserine-prothrombin complex with manifestations of the antiphospholipid syndrome and with the presence of lupus anticoagulant. Arthritis Rheum 2000;43:1982–93.
18. Wilson WA, Gharavi AE, Koike T, Lockshin MD, Branch DW, Piette JC, et al. International consensus statement on preliminary classification criteria for definite antiphospholipid syndrome: report of an international workshop. Arthritis Rheum 1999;42:1309–11.
19. Tan EM, Cohen AS, Fries JF, Masi AT, McShane DJ, Rothfield NF, et al. The 1982 revised criteria for the classification of systemic lupus erythematosus. Arthritis Rheum 1982;25:1271–7.
20. Ichikawa K, Khamashta MA, Koike T, Matsuura E, Hughes GR. β_2-glycoprotein I reactivity of monoclonal anticardiolipin antibodies from patients with antiphospholipid syndrome. Arthritis Rheum 1994;37:1453–61.
21. Matsuura E, Igarashi M, Igarashi Y, Nagae H, Ichikawa K, Yasuda T, et al. Molecular definition of human β_2-glycoprotein I (β_2-GPI) by cDNA cloning and inter-species differences of β_2-GPI in alternation of anticardiolipin binding. Int Immunol 1991;3:1217–21.
22. Matsuura E, Igarashi Y, Yasuda T, Triplett DA, Koike T. Anticardiolipin antibodies recognize β_2-glycoprotein I structure altered by interacting with an oxygen modified solid phase surface. J Exp Med 1994;179:457–62.
23. Bouma B, de Groot PG, van den Elsen JM, Ravelli RB, Schouten A, Simmelink MJ, et al. Adhesion mechanism of human β_2-glycoprotein I to phospholipids based on its crystal structure. EMBO J 1999;18:5166–74.
24. Brooks BR, Bruccoleri RE, Olafson BD, States DJ. CHARMm: a program for macromolecular energy, minimization, and dynamics calculations. J Comput Chem 1983;4:187–217.
25. Carlson W, Karplus M, Haber E. Construction of a model for the three-dimensional structure of human renal renin. Hypertension 1985;7:13–26.
26. Hirose N, Williams R, Alberts AR, Furie RA, Chartash EK, Jain RI, et al. A role for the polymorphism at position 247 of the β_2-glycoprotein I gene in the generation of anti-β_2-glycoprotein I antibodies in the antiphospholipid syndrome. Arthritis Rheum 1999;42:1655–61.
27. Prieto GA, Cabral AR, Zapata-Zuñiga M, Simón AJ, Villa AR, Alarcon-Segovia D, et al. Valine/valine genotype at position 247 of the β_2-glycoprotein I gene in Mexican patients with primary antiphospholipid syndrome: association with anti-β_2-glycoprotein I antibodies. Arthritis Rheum 2003;48:471–4.
28. Camilleri RS, Mackie IJ, Humphries SE, Machin SJ, Cohen H. Lack of association of β_2-glycoprotein I polymorphisms Val247Leu and Trp316Ser with antiphospholipid antibodies in patients with thrombosis and pregnancy complications. Br J Haematol 2003;120:1066–72.
29. Ichikawa K, Tsutsumi A, Atsumi T, Matsuura E, Kobayashi S, Hughes GR, et al. A chimeric antibody with the human γ1 constant region as a putative standard for assays to detect IgG β_2-glycoprotein I-dependent anticardiolipin and anti-β_2-glycoprotein I antibodies. Arthritis Rheum 1999;42:2461–70.
30. Tincani A, Spatola L, Prati E, Allegri F, Ferremi P, Cattaneo R, et al. The anti-β_2-glycoprotein I activity in human anti-phospholipid syndrome sera is due to monoreactive low-affinity autoantibodies directed to epitopes located on native β_2-glycoprotein I and preserved during species' evolution. J Immunol 1996;157:5732–8.
31. Saxena A, Gries A, Schwarzenbacher R, Kostner GM, Laggner P, Prassl R. Crystallization and preliminary x-ray crystallographic studies on apolipoprotein H (β_2-glycoprotein-I) from human plasma. Acta Crystallogr D Biol Crystallogr 1998;54:1450–2.
32. Ito H, Matsushita S, Tokano Y, Nishimura H, Tanaka Y, Fujisao S, et al. Analysis of T cell responses to the β_2-glycoprotein I-derived peptide library in patients with anti-β_2-glycoprotein I antibody-associated autoimmunity. Hum Immunol 2000;61:366–77.
33. Arai T, Yoshida K, Kaburagi J, Inoko H, Ikeda Y, Kawakami Y, et al. Autoreactive CD4+ T-cell clones to β_2-glycoprotein I in patients with antiphospholipid syndrome: preferential recognition of the major phospholipid-binding site. Blood 2001;98:1889–96.

THE JOURNAL OF IMMUNOLOGY

CUTTING EDGE

Cutting Edge: Fas Ligand (CD178) Cytoplasmic Tail Is a Positive Regulator of Fas Ligand-Mediated Cytotoxicity[1]

Satoshi Jodo,[2] Vyankatesh J. Pidiyar,[2†] Sheng Xiao,[†] Akira Furusaki,* Rahul Sharma,[†] Takao Koike,* and Shyr-Te Ju[3†]*

The cytotoxic function of CD178 (Fas ligand (FasL)) is critical to the maintenance of peripheral tolerance and immune-mediated tissue pathology. The active site of FasL resides at the FasL extracellular region ($FasL_{Ext}$) and it functions through binding/cross-linking Fas receptor on target cells. In this study, we report that $FasL_{Ext}$-mediated cytotoxicity is regulated by the FasL cytoplasmic tail ($FasL_{Cyt}$). Deleting the N-terminal 2–70 aa (Δ70) or N-terminal 2–33 aa (Δ33) reduced the cytotoxic strength as much as 30- to 100-fold. By contrast, change in the cytotoxic strength was not observed with FasL deleted of the proline-rich domains (45–74 aa, ΔPRD) in the $FasL_{Cyt}$. Our study identifies a novel function of $FasL_{Cyt}$ and demonstrates that $FasL_{2–33}$, a sequence unique to FasL, is critically required for the optimal expression of $FasL_{Ext}$-mediated cytotoxicity. The Journal of Immunology, 2005, 174: 4470–4474.

Fas (CD95) is a type I transmembrane protein expressed by many nucleated cells (1). The physiological ligand for Fas (FasL,[4] or CD178) is a type II transmembrane protein expressed by activated T cells and non-T cells under a variety of conditions (2, 3). The extracellular domain of FasL ($FasL_{Ext}$) has the ability to bind Fas of target cells. Cross-linking of Fas induces target cells to undergo apoptosis (4). The FasL-mediated apoptosis pathway has been implicated in peripheral tolerance (1, 2), tissue pathology (5, 6), and maintenance of the immune privileged sites (7).

FasL expression is regulated at the transcriptional, translational, and posttranslational levels. An effective way to down-regulate FasL expression is by shedding that generates soluble FasL (sFasL). Shed sFasL exhibits weak cytotoxicity and excess sFasL inhibits FasL-based, cell-mediated cytotoxicity (8). FasL is also released from cells in the form of vesicles (FasL vesicle preparation (VP)). FasL VP display full-length FasL and express strong cytotoxicity (9, 10). The physiological significance of FasL VP remains unknown.

Among TNF family members, FasL possesses a distinctive cytoplasmic tail ($FasL_{Cyt}$) of 80 aa. The sequence of $FasL_{Cyt}$ is highly conserved among species, suggesting it may have specific functions (11–14). Here, we report a novel function of $FasL_{Cyt}$. We found that $FasL_{Cyt}$ is critically required for the full expression of FasL-mediated cytotoxicity, a function associated with $FasL_{Ext}$. Compared with $FasL_{Cyt}$ deletion mutants, $FasL_{Cyt}$ enhances cytotoxicity by as much as 30- to 100-fold. In addition, we identified $FasL_{2–33}$, a unique sequence not found in other proteins, as the positive regulator of FasL-mediated cytotoxicity. Our study demonstrates a novel regulatory function of $FasL_{2–33}$ for an effector mechanism that is critically involved in various important aspects of the immune system.

Materials and Methods

Cell lines and reagents

Neuro-2a (mouse neuroblastoma), NIH-3T3 (mouse fibroblast), and COS-7 (monkey kidney fibroblast) were obtained from American Type Culture Collection (ATCC). G247.4, NOK-1 mAb, and PE-conjugated streptavidin were obtained from BD Biosciences. All restriction endonucleases were obtained from New England Biolabs. The prokaryotic expression vector pBlueScript II KS was obtained from Stratagene. The human FasL cDNA construct and the mammalian expression vector BCMGSneo were kindly provided by Dr. S. Nagata of Osaka University Medical Center (Osaka, Japan) (11).

Construction of FasL deletion mutants

The full-length human FasL cDNA cloned in pBlueScript II KS was used to generate deletion mutants by PCR using different 5′ primers and the same 3′ primer (Integrated DNA Technologies). All 5′ primers used contain the translation start sequence ATG that codes for methionine, therefore, deletion begins with amino acid residue 2 of FasL. The sequences of the 5′ primers are: 5′-ATGACCTCTGTGCCCAGAAGGCC-3′ (for Δ33 in which $FasL_{2–33}$ is deleted), 5′-ATGCTGAAGAAGAGAGGGAACCACAGC-3′ (for Δ70 in which $FasL_{2–70}$ is deleted), 5′-ATGCAGCTCTTCCACCTACAGAAG GAGC-3′ (for Δ102 in which $FasL_{2–102}$ is deleted) and 5′-GGCCTGGT CAAAGGAGGGGGAACCACAGCACAGGC-3′ (for ΔPRD (proline-rich domain deletion mutant) in which $FasL_{45–74}$ is deleted). We used Δ102 FasL together with BCMGSneo (vector control (Vc)) in every transfection experiment to control any unforeseen effect of our recombinant engineering process. The sequence of the 3′ primer is 5′-GTAAAACGACGGCCAGTGAGCG-3′ of the pBlueScript II KS. The PCR products were subcloned into pBlueScript II KS. The inserts were excised with *NotI* and *XhoI* and cloned into the BCMGSneo vector. The gene sequence of each construct was confirmed by DNA sequencing.

*Department of Medicine II, Hokkaido University Graduate School of Medicine, Sapporo, Japan; and †Division of Rheumatology and Immunology, Department of Internal Medicine, University of Virginia, Charlottesville, VA 22908

Received for publication October 13, 2004. Accepted for publication February 8, 2005.

The costs of publication of this article were defrayed in part by the payment of page charges. This article must therefore be hereby marked *advertisement* in accordance with 18 U.S.C. Section 1734 solely to indicate this fact.

[1] This work was supported in part by National Institutes of Health Grant AI36938.

[2] S.J. and V.J.P. contributed equally to this work.

[3] Address correspondence and reprint requests to Dr. Shyr-Te Ju, Division of Rheumatology and Immunology, Department of Internal Medicine, University of Virginia, Charlottesville, VA 22908-0412. E-mail address: sj8r@virginia.edu

[4] Abbreviations used in this paper: FasL, Fas ligand; $FasL_{Ext}$, FasL extracellular domain; sFasL, soluble FasL; VP, vesicle preparation; $FasL_{Cyt}$, FasL cytoplasmic tail; PRD, proline-rich domain; Vc, vector control; WT, wild type.

0022-1767/05/$02.00

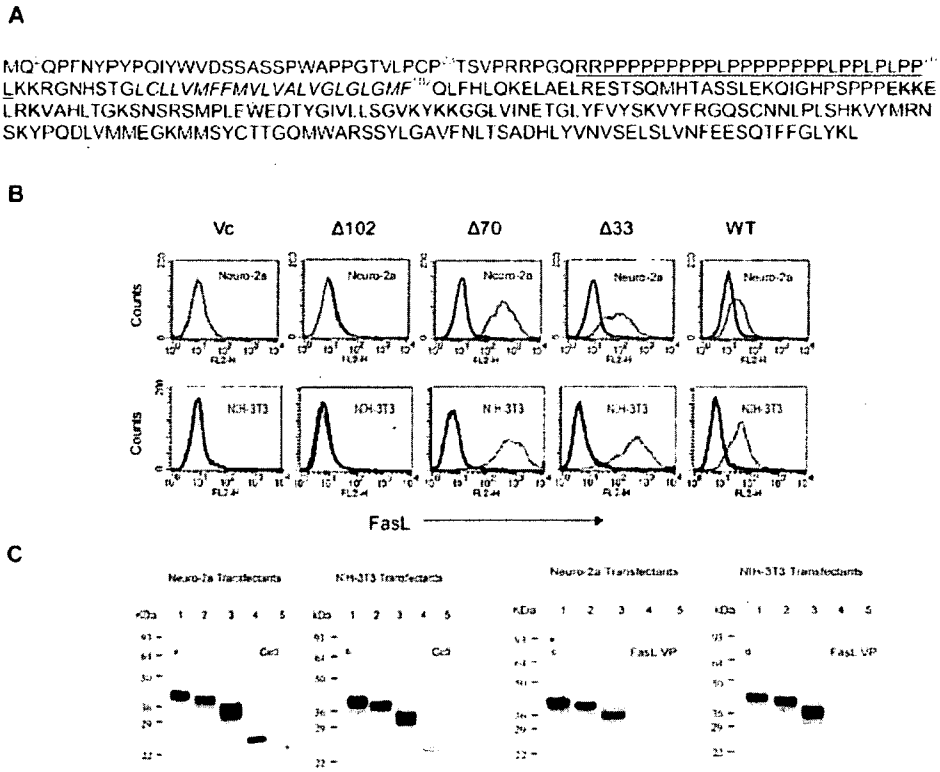

FIGURE 1. Cell surface expression of FasL by various transfectants. The WT human FasL sequence was shown in *A*. The amino acid positions 2, 33, 70, and 102 were marked to indicate the sequence deleted for Δ33 (2–33), Δ70 (2–70), and Δ102 (2–102) FasL mutants. PRD is underlined. The transmembrane domain is italicized. The strike-through sequence represents the trimerization motif. *B*, Various Neuro-2a transfectants (*upper panels*) and NIH-3T3 transfectants (*lower panels*) were stained with biotin-conjugated NOK-1 mAb (shaded area) or isotype control (open area), followed by FITC-conjugated streptavidin and analyzed with a flow cytometer. Data presented is representative of three separate experiments. *C*, Western blot analysis of FasL of various transfectants (*a* and *b*) and their FasL VP (*c* and *d*) of Neuro-2a and NIH-3T3 series. *Lanes 1–5* are samples from WT, Δ33, Δ70, Δ102, and Vc transfectants, respectively. Molecular mass markers are shown on the *left side* of each panel.

Transfection

The derivation, characterization, and culture condition for maintenance of transfectants of various cell lines have been described (15).

Flow cytometric analysis

Cells (0.5×10^6) were suspended in 0.1 ml of PBS containing 0.2% BSA and 1 μg of biotinylated NOK-1 or biotinylated control isotype. Binding reaction was conducted at 4°C for 30 min with gentle mixing periodically. Afterward, cells were washed twice with cold PBS. Bound Abs were measured by incubating with 0.5 μg of FITC-conjugated streptavidin for 30 min at 4°C. Cells were washed twice with cold PBS and then analyzed using FACScan (BD Biosciences) equipped with CellQuest software. At least 2×10^4 stained cells in the gated area were selected with each sample.

Preparation of sFasL and FasL VP

Cells at ~80% confluence were maintained in 150 mm × 25 mm petri dishes in 25 ml of culture medium for 48 h. FasL VP and sFasL were prepared as previously described (9, 10).

Table I. *FasL protein levels in various compartments of transfectant culture*[a]

	WT	Δ33	Δ70	Δ102[b]	Vc[b]
Neuro-2a[c]					
Cell lysate	3	19	89	<0.01	<0.01
FasL VP	17	14	50	<0.02	<0.02
sFasL	9	15	10	<0.2	<0.2
NIH-3T3[c]					
Cell lysate	8	65	72	<0.01	<0.01
FasL VP	31	44	54	<0.02	<0.02
sFasL	46	139	132	<0.2	<0.2

[a] FasL in samples was determined by ELISA. Data presented are representative of three separate experiments.

[b] The numbers indicate the limits of FasL detection, which depend on sample volumes used in the assay.

[c] The numbers indicate FasL total amounts in picomoles in samples. See *Materials and Methods* for sample preparation.

Quantification of FasL

The amounts of FasL in cell extract, FasL VP, and sFasL of all transfectants were determined using the $FasL_{Ext}$-specific ELISA kit (Oncogene) as previously described (10). A standard curve using recombinant sFasL provided with the kit is included in every individual assay.

Western blot analysis

Western blot analysis was conducted as previously described (9). Protein concentrations loaded were 0.1–5 μg. For samples lacking detectable FasL, 5 μg of total protein was loaded. FasL was detected using $FasL_{Ext}$-reactive G247.4 mAb followed by anti-mouse IgG-HRP (Sigma-Aldrich). Specific bands were developed using ECL (Amersham).

Cytotoxicity assay

A cytotoxicity assay was conducted as previously described using ^{51}Cr-labeled, A20 B lymphoma cells or Jurkat T lymphoma cells as targets (10). Various amounts of effector were incubated with 2×10^4 target cells for 4–8 h at 37°C in a 10% CO_2 incubator. At the end of incubation, cell-free supernatants were collected and counted with a gamma-counter (LKB). Cytotoxicity, expressed as percent-specific Cr release, was calculated by the formula: 100 × (experimental release − background release)/(total release − background release). Background release was determined by culturing target cells with medium. Total release was determined by lysing target cells with 2% Triton X-100. Experiments were conducted in duplicate and repeated at least twice.

Results and Discussion

$FasL_{Cyt}$ regulates FasL expression level

We prepared a series of FasL deletion mutant expression constructs and used them to transfect Neuro-2a and NIH-3T3 cells (Fig. 1*A*). G418-resistant transfectants were selected. We used flow cytometry to determine the cell surface expression of FasL (Fig. 1*B*). In both series of transfectants, wild-type (WT) FasL transfectants stained positive but a significantly stronger staining was observed with Δ33 and Δ70 FasL transfectants. Cell surface FasL expression was not observed with Δ102 FasL or Vc transfectants.

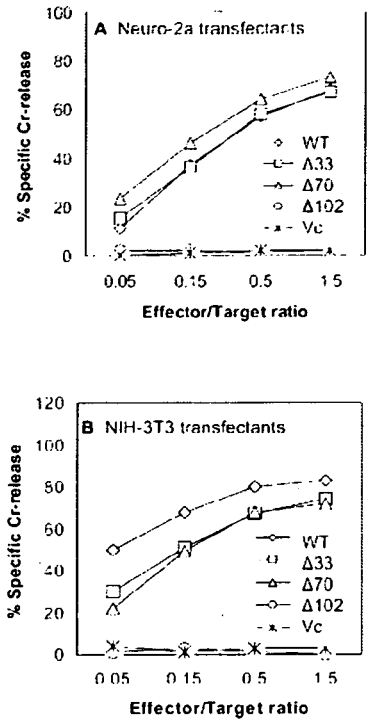

FIGURE 2. FasL-mediated cytotoxicity does not correlate with FasL membrane expression levels of transfectants. Cell-mediated cytotoxicity was conducted with various transfectants of Neuro-2a (*A*) and NIH-3T3 (*B*) series. Transfectants were cultured with ^{51}Cr-labeled Jurkat cells at various E:T ratios. The percent-specific Cr release was determined after 4 h of incubation.

We used FasL-specific ELISA to determine the total FasL levels in transfectants. Under the specific condition, WT transfectants of NIH-3T3 and Neuro-2a cell lines expressed 8 and 3 picomoles of FasL, respectively. A 6- to 30-fold increase in FasL level was observed for Δ33 FasL and Δ70 FasL transfectants. No FasL was detected in Δ102 FasL or Vc transfectants. Thus, the total FasL levels in transfectants correlated with their cell surface expression. In contrast, FasL levels in FasL VP and sFasL preparations did not correlate with the total FasL levels of transfectants (Table I). We have recently reported that the increase in FasL expression in Δ33 and Δ70 FasL transfectants is the result of an increase in the FasL translation rate (15).

We validated the size of FasL deletion mutants by Western blot analysis (Fig. 1*C*). WT, Δ33, and Δ70 FasL transfectants expressed the recombinant proteins of the predicted sizes (Fig. 1, *A* and *B*). A small size and faintly stained band was observed with the Δ102 FasL transfectant. No band was observed with Vc transfectants. FasL of predicted sizes were also observed with FasL VP prepared from the corresponding WT, Δ33, and Δ70 FasL transfectants. No band was observed with vesicles prepared from Δ102 FasL and Vc transfectants (Fig. 1*C*).

Both WT and $FasL_{Cyt}$ deletion mutants express FasL-mediated cytotoxicity

We tested these transfectants for cell-mediated cytotoxicity against the ^{51}Cr-labeled Jurkat target (Fig. 2). Cytotoxicity was not detected with Δ102 FasL and Vc transfectants. Transfectants expressing cell surface FasL displayed a dose-dependent killing based on various E:T ratios. Interestingly, the cytotoxic strength of WT FasL transfectants was comparable to that of Δ33 or Δ70 FasL transfectants despite the fact that the latter transfectants expressed significantly more FasL.

We also determined the cytotoxic strength based on the total FasL amount of transfectant using ^{51}Cr-labeled A20 B lymphoma cells as target (Fig. 3, *A* and *B*). For both series of transfectants, the cytotoxic strength of WT FasL was 10- to 30-fold stronger than that of Δ33 or Δ70 FasL transfectants. This dramatic difference is surprising because the cytotoxicity is dependent on cross-linking Fas receptors on target cells by $FasL_{Ext}$. The data therefore strongly suggest that $FasL_{Cyt}$ regulates $FasL_{Ext}$-mediated cytotoxicity across a membrane barrier. This difference in the strength of cell-mediated killing could be intrinsic to $FasL_{Cyt}$ or due to the cellular environment of FasL transfectants, or both.

Evidence from FasL VP

To firmly establish that $FasL_{Cyt}$ regulates FasL-mediated cytotoxicity, we determined the cytotoxic strength of FasL VP prepared from transfectants (Fig. 3, *C* and *D*). FasL VP is presumably a minimum subcellular component capable of expressing functional FasL transmembrane protein. It is free from sFasL. Its cytotoxicity, unlike transfectants, does not depend on protein synthesis (10). Using the same amount of FasL, FasL VP derived from WT FasL transfectants of Neuro-2a or NIH-3T3 delivered 10- to 30-fold stronger cytotoxicity than the FasL VP

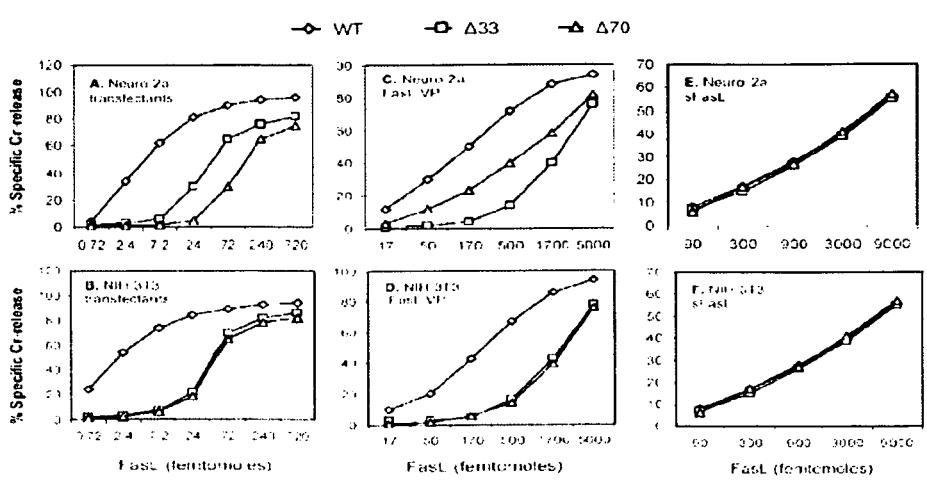

FIGURE 3. Comparison of cytotoxicity mediated by cells, FasL VP, and sFasL of various transfectants. Cells (*A* and *B*), FasL VP (*C* and *D*), and sFasL (*E* and *F*) of Neuro-2a (*A*, *C*, and *E*) and NIH-3T3 series (*B*, *D*, and *F*) were incubated with ^{51}Cr-labeled A20 target cells at various molar concentrations of FasL for 4 (cells and FasL VP) or 8 h (sFasL). Afterward, supernatants were removed and counted. The cytotoxicity data presented is representative of three experiments.

derived from Δ33 or Δ70 FasL transfectants. By contrast, the sFasL derived from these transfectants, either from Neuro-2a series (Fig. 3*E*) or from NIH-3T3 series (Fig. 3*F*), displayed nearly identical cytotoxicity. The data suggest that $FasL_{2-33}$ is important for the optimal expression of FasL-mediated cytotoxicity.

$FasL_{2-33}$ but not $FasL_{PRD}$ is required for the optimal expression of FasL-mediated cytotoxicity

$FasL_{Cyt}$ contains PRD that may interact with certain cellular proteins (12). To determine whether $FasL_{PRD}$ plays a role in FasL-mediated cytotoxicity, we generated PRD-deleted (ΔPRD) FasL transfectants from Neuro-2a and COS-7 cell lines. In contrast to Δ33 and Δ70 FasL transfectants, FasL expression was not increased in ΔPRD transfectants (data not shown). We prepared FasL VP from these transfectants and determined their cytotoxic strength (Fig. 4). For both Neuro-2a and COS-7 transfectants, the cytotoxic strength of ΔPRD FasL VP was comparable to WT FasL VP. As controls, FasL VP prepared from Δ33 FasL Neuro-2a transfectant and Δ70 FasL COS-7 transfectant displayed cytotoxicity 30- to 100-fold less than WT FasL VP. The data indicate that $FasL_{PRD}$ is not required for the optimal expression of FasL-mediated cytotoxicity. Taken together, the critical role of $FasL_{2-33}$ is demonstrated both by its deletion (as in Δ33 FasL and Δ70 FasL) that resulted in losing the $FasL_{Ext}$ cytotoxic strength and by its presence (as in ΔPRD FasL and WT FasL) that resulted in optimal display of $FasL_{Ext}$ cytotoxicity.

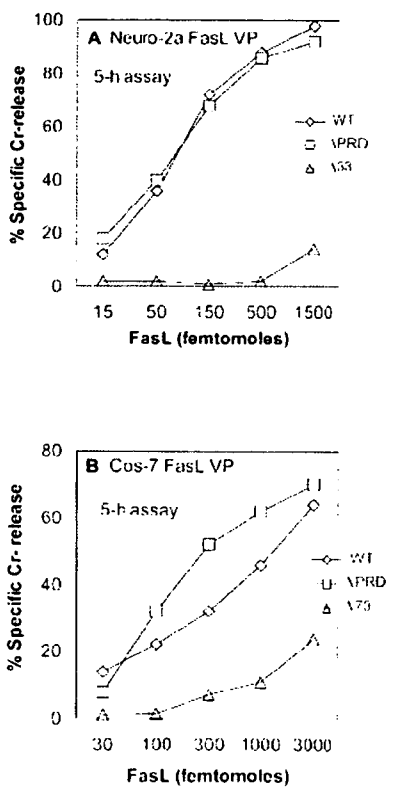

FIGURE 4. $FasL_{PRD}$ is not required for the optimal expression of FasL-mediated cytotoxicity. Samples of FasL VP were prepared from WT and ΔPRD FasL transfectants of Neuro-2a and COS-7 cell lines. FasL contents were determined using ELISA. Various amounts of FasL were compared for cytotoxic strength against ^{51}Cr-labeled A20 target. As controls, FasL VP prepared from Δ33 FasL Neuro-2a transfectant and Δ70 FasL COS-7 transfectant were analyzed in parallel. The data presented is representative of three experiments.

Our study used an artificial expression system to determine the structure and function relationship between $FasL_{Cyt}$ and $FasL_{Ext}$-mediated cytotoxicity. Deletion of $FasL_{Cyt}$ could potentially result in different localization of cell membrane FasL, change in sFasL production, faster FasL membrane movement, loss of interaction with $FasL_{Cyt}$-interacting proteins, loss of the ability to form oligomers, changes in $FasL_{Ext}$ conformation, change in phosphorylation state, etc. Additional studies are needed to determine the precise mechanism(s) and FasL-bearing vesicles offer a simple and novel system for this purpose and perhaps for other bioactive transmembrane proteins. Among these possibilities, we have ruled out the overproduction of sFasL as a mechanism for the down-regulation of cell-mediated cytotoxicity. Moreover, under the assay conditions, sFasL released were insufficient to influence the cell-mediated cytotoxicity (10). Our data further indicate that the weakened cytotoxic potential of sFasL is in part due to loss of $FasL_{Cyt}$, in addition to loss of multivalency as previously described (8). The observation that $FasL_{PRD}$ did not play a role in FasL-mediated cytotoxicity rules out the participation of potential $FasL_{PRD}$-interacting proteins such as Grb2, Grap, $p47^{phox}$, and Nck in this process (12). Moreover, no interacting protein was detected using GST-$FasL_{2-29}$ (12). These data suggest the ability to optimize FasL cytotoxicity is intrinsic to $FasL_{2-33}$. $FasL_{2-33}$ contains a DSSASSP motif that is a potential substrate for CK-I, CK-II, and GSK-3 kinases. Among them, the CK-I site (SXXS) is shared with several TNF superfamily members. Otherwise, $FasL_{2-33}$, including the Cys_{32}, a potential site for disulfide bonding and acetylation/palmitoylation, is unique among members of the TNF superfamily (⟨www.ncbi.nlm.nih.gov⟩). These properties should be helpful in determining the molecular mechanism by which the FasL-based cytotoxicity is optimized. The dramatic enhancement of cytotoxicity by $FasL_{2-33}$ may explain why FasL plays a critical role in peripheral tolerance and immune-mediated tissue damage that is dependent on cytotoxicity strength.

A regulatory role of $FasL_{Cyt}$ on $FasL_{Ext}$-mediated cytotoxicity had not been previously envisaged and our study provides the first definitive evidence supporting this novel function. Our study has significant implications with respect to regulation of membrane protein function in general and we have demonstrated this significant point in one effector function that is critically involved in peripheral tolerance, lymphocyte homeostasis, and immune-mediated tissue pathology. Our results also point out a potential complication in studies in which the cytoplasmic tail of a transmembrane protein is deleted by recombinant engineering as well as the potential use of *$FasL_{Cyt}$* and *$FasL_{2-33}$* to control the expression levels and biochemical properties of transmembrane proteins.

Acknowledgments

We thank Drs. S. M. Fu, S.-s. J. Sung, M. Brown, and T. Braciale for their critical comments and suggestions.

Disclosures

The authors have no financial conflict of interest.

References

1. Watanabe-Fukunaga, R., C. I. Brannan, N. G. Copeland, N. A. Jenkins, and S. Nagata. 1992. Lymphoproliferative disorder in mice explained by defects in Fas antigen that mediates apoptosis. *Nature 356:314.*
2. Takahashi, T., M. Tanaka, C. I. Brannan, N. A. Jenkins, N. G. Copeland, T. Suda, and S. Nagata. 1994. Generalized lymphoproliferative disease in mice, caused by a point mutation in the Fas ligand. *Cell 76:969.*
3. Bonfoco, E., P. M. Stuart, T. Brunner, T. Lin, T. S. Griffith, Y. Gao, H. Nakajima, P. A. Henkart, T. A. Ferguson, and D. R. Green. 1998. Inducible nonlymphoid expression of Fas ligand is responsible for superantigen-induced peripheral deletion of T cells. *Immunity 9:711.*
4. Rouvier, E., M.-F. Luciano, and P. Golstein. 1993. Fas involvement in Ca^{2+}-independent T cell-mediated cytotoxicity. *J. Exp. Med. 177:195.*
5. Wei, Y., K. Chen, G. C. Sharp, H. Yagita, and H. Braley-Mullen. 2001. Expression and regulation of Fas and Fas ligand on thyrocytes and infiltrating cells during induction and resolution of granulomatous experimental autoimmune thyroiditis. *J. Immunol. 167:6678.*
6. Pinkoski, M. J., T. Brunner, D. R. Green, and T. Lin. 2000. Fas and Fas ligand in gut and liver. *Am. J. Physiol. 278:G354.*
7. Griffith, T. S., X. Yu, J. M. Herndon, D. R. Green, and T. A. Ferguson. 1996. CD95-induced apoptosis of lymphocytes in an immune privileged site induces immunological tolerance. *Immunity 5:7.*
8. Tanaka, M., T. Itai, M. Adachi, and S. Nagata. 1998. Down-regulation of Fas ligand by shedding. *Nat. Med. 4:31.*
9. Strehlow, D., S. Jodo, and S.-T Ju. 2000. Retroviral membrane display of apoptotic effector molecules. *Proc. Nat. Acad. Sci. USA 97:4209.*
10. Jodo, S., S. Xiao, A. Hohlbaum, D. Strehlow, A. Marshak-Rothstein, and S.-T. Ju. 2001. Apoptosis-inducing membrane vesicles: a novel agent with unique properties. *J. Biol. Chem. 276:39938.*
11. Takahashi, T., M. Tanaka, J. Inazawa, T. Abe, T. Suda, and S. Nagata. 1994. Human Fas ligand: gene structure, chromosomal location and species specificity. *Int. Immunol. 6:1567.*
12. Ghadimi, M. P., Sanzenbacher, R. Thiede, B. Wenzel, J. Jing, Q. Plomann, M. Borkhard, A. D. Kabelitz, and O. Janssen. 2002. Identification of interaction partners of the cytosolic polyproline region of CD95 ligand (CD178). *FEBS Lett. 519:50.*
13. Suzuki, I., and P. J. Fink. 1998. Maximal proliferation of cytotoxic T lymphocytes requires reverse signaling through Fas ligand. *J. Exp. Med. 187:123.*
14. Blott, E. J., G. Bossi, R. Clark, M. Zvelebil, and G. M. Griffiths. 2001. Fas ligand is targeted to secretory lysosomes via a proline-rich domain in its cytoplasmic tail. *J. Cell Sci. 114:2405.*
15. Xiao, S., U. S. Deshmukh, S. Jodo, T. Koike, R. Sharma, R. Furusaki, S-s. J. Sung, and S-T. Ju. 2004. Novel negative regulator of expression in Fas ligand (CD178) cytoplasmic tail: evidence for translational regulation and against FasL retention in secretory lysosomes. *J. Immunol. 173:5095.*

Pkd1 regulates immortalized proliferation of renal tubular epithelial cells through p53 induction and JNK activation

Saori Nishio,[1,2] Masahiko Hatano,[2] Michio Nagata,[3] Shigeo Horie,[4] Takao Koike,[1] Takeshi Tokuhisa,[2] and Toshio Mochizuki[1]

[1]Department of Medicine II, Hokkaido University Graduate School of Medicine, Sapporo, Japan. [2]Department of Developmental Genetics (H2), Graduate School of Medicine, Chiba University, Chiba, Japan. [3]Department of Pathology, Institute of Basic Medical Sciences, University of Tsukuba, Tsukuba, Japan. [4]Department of Urology, Teikyo University School of Medicine, Tokyo, Japan.

Autosomal dominant polycystic kidney disease (ADPKD) is the most common human monogenic genetic disorder and is characterized by progressive bilateral renal cysts and the development of renal insufficiency. The cystogenesis of ADPKD is believed to be a monoclonal proliferation of PKD-deficient (*PKD*$^{-/-}$) renal tubular epithelial cells. To define the function of *Pkd1*, we generated chimeric mice by aggregation of *Pkd1*$^{-/-}$ ES cells and *Pkd1*$^{+/+}$ morulae from ROSA26 mice. As occurs in humans with ADPKD, these mice developed cysts in the kidney, liver, and pancreas. Surprisingly, the cyst epithelia of the kidney were composed of both *Pkd1*$^{-/-}$ and *Pkd1*$^{+/+}$ renal tubular epithelial cells in the early stages of cystogenesis. *Pkd1*$^{-/-}$ cyst epithelial cells changed in shape from cuboidal to flat and replaced *Pkd1*$^{+/+}$ cyst epithelial cells lost by JNK-mediated apoptosis in intermediate stages. In late-stage cysts, *Pkd1*$^{-/-}$ cells continued immortalized proliferation with downregulation of p53. These results provide a novel understanding of the cystogenesis of ADPKD patients. Furthermore, immortalized proliferation without induction of p53 was frequently observed in 3T3-type culture of mouse embryonic fibroblasts from *Pkd1*$^{-/-}$ mice. Thus, *Pkd1* plays a role in preventing immortalized proliferation of renal tubular epithelial cells through the induction of p53 and activation of JNK.

Introduction

Autosomal dominant polycystic kidney disease (ADPKD) is the most common human monogenic genetic disorder and is characterized by progressive bilateral renal enlargement with numerous cysts and fibrosis in the renal parenchyma. It is often accompanied by extra-renal manifestations, such as hypertension, intracranial aneurysms, and hepatic and pancreatic cysts (1). The disease is progressive, and many patients develop renal insufficiency in the fifth and sixth decades of life. Cystogenesis has been studied by microdissection of ADPKD kidneys. The initial event in cyst formation is believed to be the dilatation and "out-pocketing" of tubules. The cysts arise from any segment of one nephron and maintain continuity with the "parental" nephron (2). Fully developed cysts are apparently isolated from the "parental" nephron and expand through the accumulation of cyst fluid (3).

The *PKD1* gene (encoding polycystin-1) (4) and the *PKD2* gene (encoding polycystin-2) (5) have been identified by positional cloning as being the genes responsible for ADPKD. Loss of heterozygosity or second somatic mutations at the *PKD1* or *PKD2* loci have been reported in cystic epithelia from ADPKD patients (6–10). Several lines of mice in which the *Pkd1* or *Pkd2* gene was targeted show similar phenotypes. Although heterozygous knockout mice develop renal and hepatic cysts later in life (after age 16 months) (11), those mice do not fully recapitulate the severity of human ADPKD. Homozygous knockout mice die in utero and develop severely polycystic kidneys (12–16). Interestingly, compound heterozygous *Pkd2*$^{WS25/-}$ mice, which carry a unique *Pkd2* allele that is prone to genomic rearrangement leading to a null allele, develop severely polycystic kidneys during adulthood and thus resemble the ADPKD phenotypes (12). These model animals suggested that a "2-hit" mechanism at either the *PKD1* or *PKD2* gene explains the late onset of the disease as well as some of the variation in clinical symptoms (17, 18).

The molecular mechanisms of the cyst formation of Pkd-deficient (*Pkd*$^{-/-}$) renal tubular epithelial cells have been studied extensively. Polycystin-1 and polycystin-2 are localized in the primary cilium of renal tubular epithelial cells (19). The relationship between cystogenesis and the disruption of cilia has been reported (20, 21). Although polycystin-2 in node monocilia contributes to the development of left-right asymmetry (22), polycystin-1 and polycystin-2 in the primary cilium transduce the extracellular mechanical stimulus induced by urinary flow into increases in cytosolic Ca^{2+}, which may regulate renal tube size (19, 23).

The cyst epithelial cells of ADPKD kidneys have a high mitotic rate in vitro (24) and in vivo, as detected by immunostaining for proliferating cell nuclear antigen (PCNA) (25), c-Myc, and Ki-67 (26). Their high mitotic rate has also been supported by the following results. First, expression of growth factors such as EGF and their receptors increases in ADPKD cysts (3, 27). Second, cAMP stimulates the in vitro proliferation of ADPKD cyst epithelium and cyst growth (28, 29). Third, overexpression of the *Pkd1* gene in a cell line induced cell cycle arrest at the G0/G1 phase with upregulation of p21 through activation of the JAK-STAT pathway (30). Thus, the proliferation of a *PKD*$^{-/-}$ cyst epithelial cell might explain the cystogenesis of ADPKD kidneys. However, polycystin-1

Nonstandard abbreviations used: ADPKD, autosomal dominant polycystic kidney disease; DBA, *Dolichos biflorus* agglutinin; LZ, LacZ; MEF, mouse embryonic fibroblast; p-, phosphorylated; PCNA, proliferating cell nuclear antigen.

Conflict of interest: The authors have declared that no conflict of interest exists.

Citation for this article: *J. Clin. Invest.* **115**:910–918 (2005). doi:10.1172/JCI200522850.

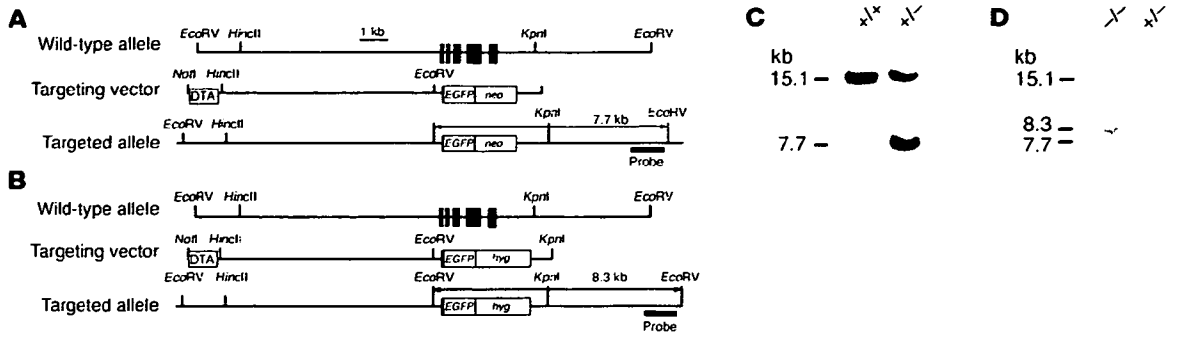

Figure 1

Generation of *Pkd1*$^{-/-}$ ES cells. (**A** and **B**) Genomic organization of 2 targeting vectors. Exons are depicted as filled boxes. The targeting vectors were designed to replace a DNA segment of exons 2–6 by a neomycin-resistance gene cassette (*neo*) (**A**) or a hygromycin-resistance gene cassette (*hyg*) (**B**). *EGFP*, gene encoding enhanced GFP. (**C** and **D**) Southern blots of genomic DNA derived from ES clones. Purified DNA was digested with *Eco*RV and bands were detected by a probe, as described in Methods. Fragments corresponding to wild-type (15.1 kb) and targeted (7.7 kb and 8.3 kb) alleles are shown. +/+, wild-type; –/–, *Pkd1*$^{-/-}$.

and polycystin-2 can be detected in some of the cyst epithelial cells of ADPKD kidneys (31–36). These results suggest a contribution of normal renal tubular epithelial cells to cystogenesis.

The cystogenesis of ADPKD kidneys cannot be fully reproduced in the kidneys of *Pkd1*$^{-/-}$ mice, because these mice die in utero and their renal tubular epithelial cells are not mosaic for *Pkd1*$^{-/-}$ and normal cells, as are ADPKD kidneys. In an attempt to establish an animal model for human ADPKD, we generated chimeric mice by an aggregation method using *Pkd1*$^{-/-}$ ES cells and normal morulae from LacZ^{+} (LZ^{+}) ROSA26 mice (37). We show here that chimeric mice with a low degree of chimerism survived for more than 1 month and had multiple cysts not only in the kidneys but also in the liver and pancreas, suggesting this may be a feasible model for human ADPKD. Surprisingly, both *Pkd1*$^{-/-}$ and wild-type (LZ^{+}) epithelial cells were involved in early cystogenesis in kidneys of the chimeric mice. We discuss here the molecular mechanisms of the cystogenesis of *Pkd1*$^{-/-}$ and *Pkd1*$^{+/+}$ renal tubular epithelial cells.

Results

Cystogenesis of Pkd1$^{-/-}$*/LZ*$^{+}$ *chimeric mice.* We generated mice carrying a mutation in the *Pkd1* gene using standard gene-targeting procedures by replacing exons 2–6 with the neomycin-resistance gene (Figure 1A). Homozygous mutant (*Pkd1*$^{-/-}$) mice died in utero with severely polycystic kidneys and cardiac abnormalities (data not shown), similar to previous descriptions (14, 15). A second targeting vector with the hygromycin-resistance gene (Figure 1B) was transfected into heterozygous (*Pkd1*$^{+/-}$) ES cells to obtain *Pkd1*$^{-/-}$ ES cells. Each gene targeting was confirmed by Southern blot (Figure 1, C and D). Then, we generated chimeric mice composed of mixtures of *Pkd1*$^{-/-}$ and wild-type cells. To monitor cells derived from *Pkd1*$^{-/-}$ ES cells in chimeric mice, we used morulae from LZ^{+} ROSA26 mice. Four independently targeted *Pkd1*$^{-/-}$ ES clones were aggregated with ROSA26 morulae to generate *Pkd1*$^{-/-}$/LZ^{+} chimeric mice.

Several *Pkd1*$^{-/-}$/LZ^{+} mice survived beyond 1 month of age, and their survival closely depended on the degree of chimerism, as estimated by coat color. When the contribution of *Pkd1*$^{-/-}$ ES cells to coat color was more than 30%, the chimeric mice either died in utero or died by P7 with severely polycystic kidneys. *Pkd1*$^{-/-}$/LZ^{+} mice with a lower contribution (less than 10%) of *Pkd1*$^{-/-}$ ES cells to their coat color survived beyond 1 month of age. Renal cysts were detected in all the *Pkd1*$^{-/-}$/LZ^{+} mice examined (n = 90). When we compared chimerism and cyst formation in P7 *Pkd1*$^{-/-}$/LZ^{+} kidneys, the incidence of cysts roughly correlated with the degree of chimerism (Figure 2, A and B). *Pkd1*$^{-/-}$/LZ^{+} kidneys were enlarged due to scattered tubular cysts observed in both the cortex and the outer medulla. These cysts occupied roughly 20–90% of the cut surface of the kidneys, in parallel with the degree of chimerism. A P60 *Pkd1*$^{-/-}$/LZ^{+} mouse had bilateral enlarged kidneys deformed by many cysts and often accompanied by hemorrhage (Figure 2C). Cut surfaces of the kidney showed little renal parenchyma (Figure 2D). This mouse also exhibited hepatic and pancreatic cysts. These pathological findings in *Pkd1*$^{-/-}$/LZ^{+} mice with low degree of chimerism were similar to those of human ADPKD.

To examine initial cyst formation in kidneys of *Pkd1*$^{-/-}$/LZ^{+} and *Pkd1*$^{-/-}$ mice, we microdissected a single nephron from the kidneys of those mice at E17.5. As shown in Figure 2E, multiple "out-pocketing" cysts were observed in all segments of the nephron from *Pkd1*$^{-/-}$/LZ^{+} mice, whereas cysts in the nephrons from *Pkd1*$^{-/-}$ mice were confined mainly to the distal tubule. Surprisingly, the cyst epithelia in chimeric mice were composed of not only *Pkd1*$^{-/-}$ cells but also LZ^{+} wild-type cells, as detected by β-gal staining (Figure 2F). Histochemical examination also showed the presence of LZ^{+} wild-type cells in the cyst epithelia of *Pkd1*$^{-/-}$/LZ^{+} kidneys (Figure 2G).

Dedifferentiation of cyst epithelial cells in Pkd1$^{-/-}$*/LZ*$^{+}$ *mice.* Cystogenesis in kidneys of *Pkd1*$^{-/-}$/LZ^{+} mice with low degree of chimerism was analyzed histologically between P1 and P30. At the early stage (P1), small cysts were numerous and their cyst epithelia were composed of many LZ^{+} cells and some *Pkd1*$^{-/-}$ cells (Figure 3A). At the late stage (P30), individual cysts were enlarged and most of the cyst epithelia were composed of *Pkd1*$^{-/-}$ cells. Similar histological findings were observed in the livers of *Pkd1*$^{-/-}$/LZ^{+} mice (data not shown). Morphological analysis of cyst epithelial cells at the early stage of cystogenesis demonstrated that many of the cyst epithelial *Pkd1*$^{-/-}$ and LZ^{+} cells were cuboidal in shape (Figure 3B). Although the shape of LZ^{+} cyst epithelial cells was still cuboidal at the intermediate stage of cystogenesis, many *Pkd1*$^{-/-}$ cyst epithelial cells changed their shape from cuboidal to flat (Figure 3C), suggesting that flat cyst epithelial cells are dedifferentiated.

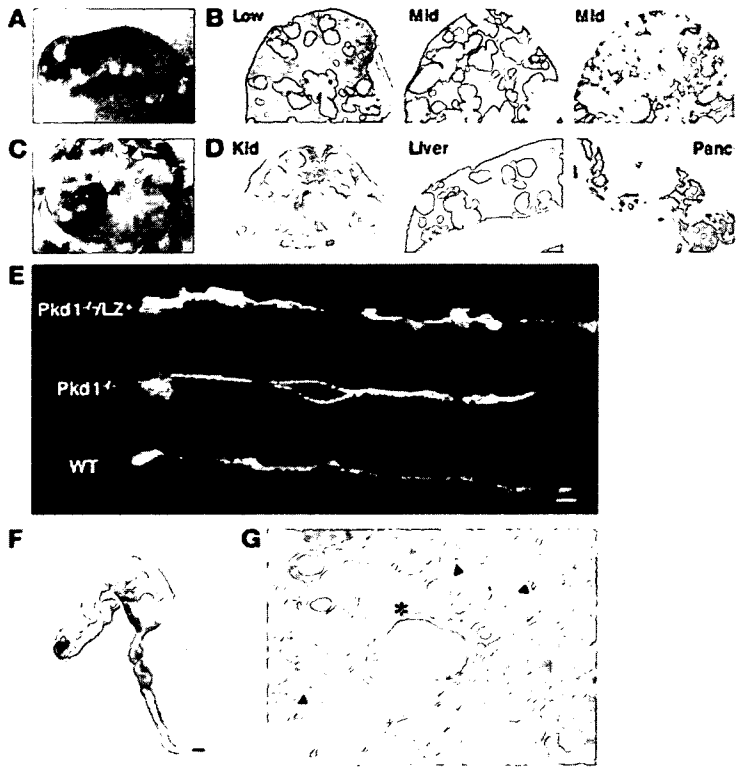

Figure 2
Pkd1$^{-/-}$/LZ^{+} mice as an animal model of human ADPKD. (**A**) Appearance of a P7 *Pkd1*$^{-/-}$/LZ^{+} mouse with an intermediate chimeric rate. The chimeric rate was estimated by coat color. (**B**) Kidneys of P7 *Pkd1*$^{-/-}$/LZ^{+} mice. Low and Mid (intermediate) indicate the chimeric rate as estimated by coat color: Low, less than 10%; Mid, 10% to approximately 30%. (**C**) Kidneys of a P60 *Pkd1*$^{-/-}$/LZ^{+} mouse. Black arrowheads indicate hemorrhagic cysts; white arrowhead indicates pancreatic cysts. (**D**) Cross sections of kidney (Kid), liver, and pancreas (Panc) of a P60 *Pkd1*$^{-/-}$/LZ^{+} mouse. Approximately 90% of the renal parenchyma is occupied by large cysts (PAS staining). Liver and pancreas show numerous cysts (H&E). Original magnification, ×2 (kidney) and ×2.5 (liver and pancreas). (**E**) Single nephrons of *Pkd1*$^{-/-}$/LZ^{+}, *Pkd1*$^{-/-}$, and wild-type mice at E17.5. Multiple "out-pocketing" cysts are present in all segments of the nephron from the *Pkd1*$^{-/-}$/LZ^{+} mouse. Cystic dilation begins at the distal tubule of the nephron of the *Pkd1*$^{-/-}$ mouse. Scale bar: 100 μm. (**F**) Staining of a microdissected tubule with β-gal. A cystic fragment of the *Pkd1*$^{-/-}$/LZ^{+} mouse was composed of *Pkd1*$^{+/+}$ (blue; LZ^{+}) and *Pkd1*$^{-/-}$ (white; LZ^{-}) cells. Scale bar: 100 μm. (**G**) Histochemical analysis of the kidney of a *Pkd1*$^{-/-}$/LZ^{+} mouse at E17.5 with β-gal. The cyst (*) began at tubules involving *Pkd1*$^{-/-}$ (LZ^{-}) and LZ^{+} cells. Some tubules composed of LZ^{-} cells (black arrowheads) showed no cystic dilatation. Counterstaining: Nuclear Fast Red. Original magnification, ×400.

To examine dedifferentiation of flat cyst epithelial cells, we examined expression of polycystin-2 and acetylated tubulin as a marker of primary cilia in the cyst epithelial cells of *Pkd1*$^{-/-}$/LZ^{+} kidneys. All of the cyst epithelial cells expressed polycystin-2 regardless of morphological changes and *Pkd1* expression (Figure 4A), and both LZ^{+} and *Pkd1*$^{-/-}$ (LZ^{-}) cyst epithelial cells manifested cilia (Figure 4B). However, some of the cyst epithelial cells had lost expression of *Dolichos biflorus* agglutinin (DBA) lectins (Figure 4C) and Na-K ATPase (Figure 4D). The loss of expression did not correlate with loss of the *Pkd1* gene in cyst epithelial cells. The mean cell height of cyst epithelial cells with or without Na-K ATPase was lower than that of normal epithelial cells ($P < 0.001$), and the cell height of cyst epithelial cells without Na-K ATPase was slightly lower than that of cyst epithelial cells with Na-K ATPase ($P = 0.029$) (Figure 4E), indicating a tendency of correlation between the dedifferentiation and the flat shape of cyst epithelial cells.

Proliferation and apoptosis of cyst epithelial cells. Immunohistochemistry of cyst epithelial cells in *Pkd1*$^{-/-}$/LZ^{+} kidneys revealed that LZ^{+} cells occasionally showed focal hyperplastic features (Figure 5A) such as micropolyps, as observed in human ADPKD. Some of cuboidal cyst epithelial cells were accompanied by PCNA expression (Figure 5B). We investigated expression of the cell cycle regulators p21 and p53 in *Pkd1*$^{-/-}$/LZ^{+} kidneys by Western blot. Although very low expression of p21 has been reported in the whole body of *Pkd1*$^{-/-}$ embryos at E15.5 (30), the amount of p21 in the kidneys of *Pkd1*$^{-/-}$ embryos at E16.5 and *Pkd1*$^{-/-}$/LZ^{+} mice 1 month of age was slightly less than that in wild-type mice (Figure 5C). Statistical analysis of the amount of p21 in 4 independent experiments indicated a significant difference between wild-type kidneys and *Pkd1*$^{-/-}$ kidneys ($P = 0.016$) but no difference between wild-type kidneys and *Pkd1*$^{-/-}$/LZ^{+} kidneys ($P = 0.107$). Interestingly, the amount of p53 in *Pkd1*$^{-/-}$ ($P = 0.003$) and *Pkd1*$^{-/-}$/LZ^{+} ($P = 0.044$) kidneys was reduced compared with that in wild-type kidneys. Indeed, the amount of p53 decreased in the cuboidal cyst epithelial cells as well as in the flat cyst epithelial cells of *Pkd1*$^{-/-}$/LZ^{+} kidneys (Figure 5D).

To examine the proliferation of cyst epithelial cells in vitro, we cultured microdissected single nephrons with cysts from *Pkd1*$^{-/-}$/LZ^{+} kidneys in collagen gel with 10% FCS. Cells in cystically dilated parts of the nephrons rapidly proliferated in a sheet-like fashion within 18 hours (Figure 5, E-G). Although the great majority were *Pkd1*$^{-/-}$ cells, some LZ^{+} cyst epithelial cells proliferated. This significant proliferation of *Pkd1*$^{-/-}$ and LZ^{+} cyst epithelial cells was sustained by FCS, as a less significant proliferation was observed in collagen gel without FCS (data not shown).

Cyst epithelia at the early stage of cystogenesis were composed of cuboidal *Pkd1*$^{-/-}$ and LZ^{+} cells in *Pkd1*$^{-/-}$/LZ^{+} kidneys, then flat *Pkd1*$^{-/-}$ cells became dominant in cyst epithelia at the intermediate stage. As there were many apoptotic cells present in *Pkd1*$^{-/-}$/LZ^{+} kidneys at the intermediate stage (data not shown), the cuboidal LZ^{+} cells in the cyst epithelia might have been dead due to apoptosis and then filled with flat *Pkd1*$^{-/-}$ cells. Indeed, TUNEL staining of the cyst epithelial cells in *Pkd1*$^{-/-}$/LZ^{+} kidneys revealed scattered TUNEL-positive cells (Figure 6A). Apoptosis in LZ^{+} cyst epithelial cells was 3- to 4-fold larger than that in *Pkd1*$^{-/-}$ cyst epithelial cells (Figure 6B). Electron microscopic analysis of the cyst epithelia showed occasional apoptotic figures in cuboidal cells overlaid by neighboring cells (Figure 6C). In addition, flat cells overlaid several degenerated cells that were detached from the tubular basement membrane (Figure 6D), suggesting rearrangement by flat *Pkd1*$^{-/-}$ cells.

Signaling pathways in relation to proliferation or apoptosis of cyst epithelial cells. Signaling pathways related to cell proliferation were analyzed in the kidneys of *Pkd1*$^{-/-}$ and *Pkd1*$^{-/-}$/LZ^{+} mice. Phosphorylated EGFR (p-EGFR) detected in the cyst epithelial cells of *Pkd1*$^{-/-}$/LZ^{+} kidneys was significantly greater than in those of wild-type kidneys

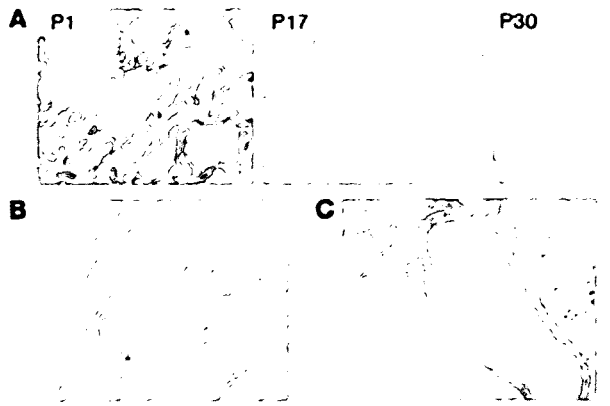

Figure 3
Histochemical analysis of *Pkd1*$^{-/-}$/LZ^{+} kidneys. Kidneys of *Pkd1*$^{-/-}$/LZ^{+} mice were stained with β-gal and counterstained with Nuclear Fast Red. **(A)** Kidneys of *Pkd1*$^{-/-}$/LZ^{+} mice with the low chimeric rate at P1, P17, and P30. At the early stage (P1), cyst epithelia were composed of *Pkd1*$^{-/-}$ (LZ^{-}) and LZ^{+} cells. At the late stage (P30), individual cysts were enlarged and most cyst epithelia were composed of *Pkd1*$^{-/-}$ (LZ^{-}) cells. Original magnification, ×200. **(B)** Kidney of a P3 *Pkd1*$^{-/-}$/LZ^{+} mouse with the intermediate chimeric rate. At the early stage of cystogenesis, both *Pkd1*$^{-/-}$ (LZ^{-}) and LZ^{+} cyst epithelial cells are cuboidal in shape. Original magnification, ×400. **(C)** Kidney of a P8 *Pkd1*$^{-/-}$/LZ^{+} mouse with the low chimeric rate. Cyst epithelia are composed of flat *Pkd1*$^{-/-}$ (LZ^{-}) cells and cuboidal LZ^{+} cells. *Pkd1*$^{-/-}$ (LZ^{-}) cyst epithelial cells changed their shape from cuboidal to flat. Original magnification, ×200.

(data not shown). To elucidate the downstream signaling pathway of growth factors, we analyzed the amount of activated MAP kinases in kidneys using Western blot and immunohistochemistry. Although the amount of p-ERK in *Pkd1*$^{-/-}$ and *Pkd1*$^{-/-}$/LZ^{+} kidneys was not different from that in wild-type kidneys (Figure 7A), expression of p-ERK was significantly more in the cyst epithelial cells of *Pkd1*$^{-/-}$/LZ^{+} kidneys regardless of their shape, cuboidal (Figure 7B) or flat (data not shown).

As for signaling pathways related to apoptosis, the amount of p-JNK was more in *Pkd1*$^{-/-}$/LZ^{+} kidneys (P = 0.046) but less in *Pkd1*$^{-/-}$ kidneys (P = 0.002) than in wild-type kidneys. Immunohistochemistry revealed that p-JNK expression was increased in the cuboidal cyst epithelial cells rather than in the flat ones of *Pkd1*$^{-/-}$/LZ^{+} kidneys, suggesting that LZ^{+} cyst epithelial cells with p-JNK expression induce apoptosis. In contrast, the amount of p-p38 in *Pkd1*$^{-/-}$/LZ^{+} and *Pkd1*$^{-/-}$ kidneys was similar to that in wild-type kidneys. Furthermore, the amount of p-Akt, an apoptotic inhibitory signal, in both *Pkd1*$^{-/-}$ (P = 0.008) and *Pkd1*$^{-/-}$/LZ^{+} (P = 0.037) kidneys was more than that in wild-type kidneys. Indeed, p-Akt expression was significantly increased in both cuboidal (data not shown) and flat cyst epithelial cells. The amount of Bcl-X_L in *Pkd1*$^{-/-}$/LZ^{+} kidneys was clearly less than that in wild-type kidneys (P = 0.032), whereas that in *Pkd1*$^{-/-}$ kidneys was similar to that in wild-type kidneys. The amount of Bcl-2 and Bax in *Pkd1*$^{-/-}$/LZ^{+} and *Pkd1*$^{-/-}$ kidneys was similar to that in wild-type kidneys (P = 0.224 and 0.821, respectively). These findings suggest that LZ^{+} cyst epithelial cells are more apoptotic than are *Pkd1*$^{-/-}$ cyst epithelial cells.

Immortalized growth of Pkd1$^{-/-}$ *mouse embryonic fibroblasts.* Most cyst epithelial cells in *Pkd1*$^{-/-}$/LZ^{+} kidneys at the late stage of cystogenesis were *Pkd1*$^{-/-}$ cells, and these grew very well in collagen gel, suggesting a relationship between loss of *Pkd1* and cell immortalization. Because the 3T3 culture protocol of mouse embryonic fibroblasts (MEFs) is one of the well characterized experimental models of cell immortalization (38) and because normal MEFs express *Pkd1* (data not shown), we cultured *Pkd1*$^{-/-}$ MEFs according to the 3T3 protocol. Wild-type MEFs entered a characteristic cell cycle arrest known as cell senescence after passages 8–9 and immortalized cells (2 of 21 wells) appeared stochastically and eventually overtook the senescent cells (Figure 8A). In contrast, immortalized cells appeared in a large number of wells (21 of 24 wells) in *Pkd1*$^{-/-}$ MEF cultures, thereby suggesting a high incidence of immortalization.

Because the amount of the cell cycle regulator p16 increases in MEFs at the senescence stage (39), we analyzed expression of the cell cycle regulators p16, p21, and p53 in *Pkd1*$^{-/-}$ MEFs using Western blot. The amount of these proteins was similar in *Pkd1*$^{-/-}$ and wild-type MEFs until passage 8, whereas the amount of p16 clearly increased in both *Pkd1*$^{-/-}$ and wild-type MEFs after passage 8 (Figure 8B). However, the amount of p53 in *Pkd1*$^{-/-}$ MEFs at pas-

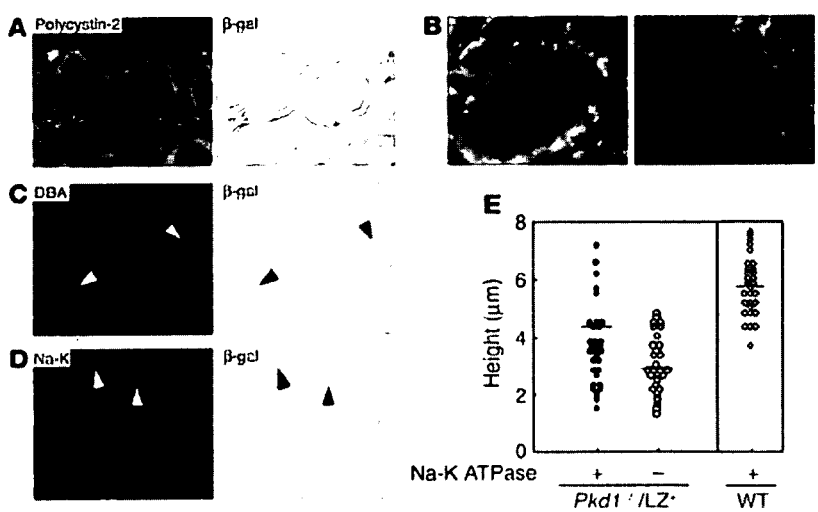

Figure 4
Dedifferentiation of *Pkd1*$^{-/-}$ cyst epithelial cells. **(A–D)** A kidney from a P8 *Pkd1*$^{-/-}$/LZ^{+} mouse was stained with anti–polycystin-2 (red, polycystin-2; blue, DAPI) **(A)**, anti–acetylated tubulin (red, acetylated tubulin; green, β-gal; blue, DAPI) **(B)**, anti-DBA **(C)** or anti–Na-K ATPase **(D)**. (Right panels: **A**, **C**, and **D**) The same section was stained with β-gal and counterstained with Nuclear Fast Red. White and black arrowheads indicate the same epithelial cells. Original magnification, ×400. **(B)** Left and right panels indicate stainings in cuboidal and flat cyst epithelia, respectively. **(E)** Relationship between cell height and Na-K ATPase expression in the cyst epithelial cells shown in **D**. Each symbol indicates a cyst epithelial cell (*Pkd1*$^{-/-}$/LZ^{+}) or normal tubular epithelial cell (WT).

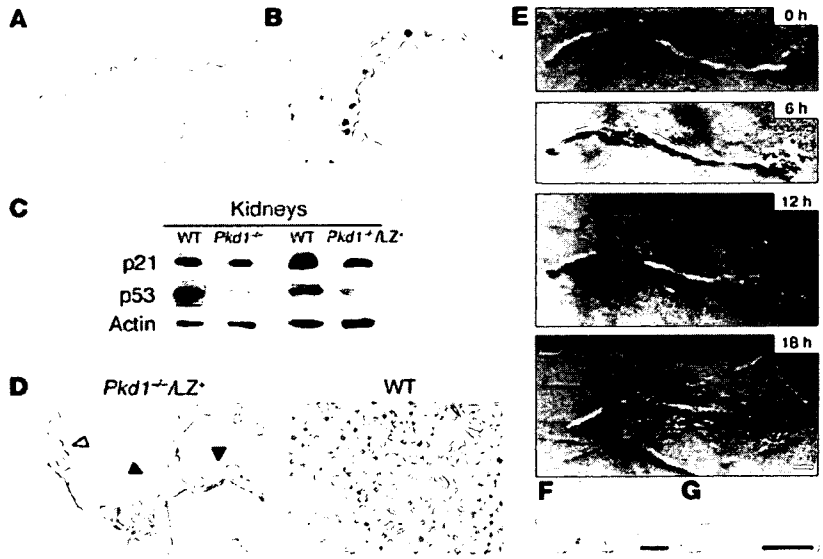

Figure 5

Proliferation of *Pkd1*$^{-/-}$ cyst epithelial cells. (**A**) A kidney from a P17 *Pkd1*$^{-/-}$/LZ^{+} mouse was stained with β-gal and counterstained with Nuclear Fast Red. LZ^{+} epithelial cells occasionally showed focal hyperplastic features such as micropolyps. Original magnification, ×400. (**B**) A kidney froma P12 *Pkd1*$^{-/-}$/LZ^{+} mouse was stained with an anti-PCNA. Some cuboidal LZ^{+} cyst epithelial cells were accompanied by PCNA expression. Original magnification, ×400. (**C**) Expression of p21 and p53 in the kidneys of *Pkd1*$^{-/-}$ mice at E16.5 and *Pkd1*$^{-/-}$/LZ^{+} mice 1 month of age. The amount of p21 and p53 in kidneys was examined using Western blot. Actin was used as a loading control for protein. Data presented are 1 representative of 4 independent experiments. (**D**) Kidneys of P12 *Pkd1*$^{-/-}$/LZ^{+} and P12 wild-type mice were stained with anti-p53. Expression of p53 was detected in the flat epithelial cells (white arrowhead) but was significantly decreased in the cuboidal cyst epithelial cells (black arrowheads) of the *Pkd1*$^{-/-}$/LZ^{+} mouse. Original magnification, ×400. (**E–G**) The proliferation of cyst epithelial cells in vitro. A single nephron isolated by microdissection from the kidney of a *Pkd1*$^{-/-}$/LZ^{+} mouse at E17.5 was cultured in collagen gel for 18 hours. (**F** and **G**) Higher magnifications of the boxed area above. Both LZ^{+} and *Pkd1*$^{-/-}$ (LZ^{-}) cells proliferated. Scale bars: 100 μm.

sage 30 ($P = 0.001$) but not that in wild-type MEFs at passage 13 ($P = 0.636$) was clearly less than that in *Pkd1*$^{-/-}$ and wild-type MEFs at passage 1. The amount of activated MAP kinases in MEFs was examined further. The amount of p-ERK in *Pkd1*$^{-/-}$ MEFs at passage 30 was slightly more than that in wild-type MEFs at passage 13. Although the amount of p-JNK ($P = 0.032$) and p-p38 ($P = 0.038$) increased in wild-type MEFs from passage 8 to passage 13, it was stable in *Pkd1*$^{-/-}$ MEFs until passage 30. The amount of p-Akt in *Pkd1*$^{-/-}$ MEFs was also stable until passage 30. Furthermore, the amount of Bcl-2 family proteins was similar in *Pkd1*$^{-/-}$ and wild-type MEFs at passages 30 and 13, respectively (data not shown).

Discussion

In the present study, we developed *Pkd1*$^{-/-}$/LZ^{+} chimeric mice. The pathological findings in *Pkd1*$^{-/-}$/LZ^{+} kidneys were similar to those in human ADPKD kidneys. Therefore, *Pkd1*$^{-/-}$/LZ^{+} mice, like *Pkd2*$^{WS25/-}$ mice (12), are a feasible model for human ADPKD. As intragenic recombination events in *Pkd2*$^{WS25/-}$ mice occurred gradually and postnatally, as in human ADPKD, whereas *Pkd1*$^{-/-}$/LZ^{+} mice have *Pkd1*$^{-/-}$ cells by inheritance, cyst formation in *Pkd1*$^{-/-}$/LZ^{+} kidneys progressed more rapidly than that in *Pkd2*$^{WS25/-}$ and human ADPKD kidneys. However, with *Pkd1*$^{-/-}$/LZ^{+} mice, we have the advantage of distinguishing *Pkd1*$^{-/-}$ cells from normal (LZ^{+}) cells and of monitoring the contribution of *Pkd1*$^{-/-}$ cells in cystogenesis. Analyses of the cyst epithelial cells in *Pkd1*$^{-/-}$/LZ^{+} kidneys can help us to understand the in vivo effect of polycystin-1 on cystogenesis.

Proliferation of normal tubular epithelial cells in early cystogenesis. Cystogenesis in human ADPKD has been proposed as being a monoclonal proliferation of PKD1- or PKD2-deficient epithelial cells (6–10). However, we found that the cystic epithelium at the early stage of cystogenesis was composed of both *Pkd1*$^{-/-}$ and LZ^{+} wild-type cells. This finding is supported by results showing that expression of polycystin-1 and polycystin-2 was detected in most cultured cells derived from ADPKD kidneys (40). We stress that the strong expression of polycystin-1 and polycystin-2 on cystic epithelia in ADPKD kidneys (31–36) may reflect involvement of normal cyst epithelial cells in the cystogenesis of human ADPKD.

The initial cystogenesis in the kidney with *Pkd1*$^{-/-}$ tubular epithelial cells requires stimulation, as some of the tubules with *Pkd1*$^{-/-}$ epithelial cells occasionally had no cystic dilatation and metanephric culture of organs harvested from *Pkd1*$^{-/-}$ mice at E13.5 failed to show cyst development (data not shown). It has been suggested that urinary flow promotes nephron development, in particular, tubular elongation with cell differentiation (41). During nephron development, it is hypothesized that the renal tubular diameter is maintained at the proper size (23) and that the primary cilium affects the maintenance of the tubular diameter by its mechanosensor function (19, 20). Cilia structure and polycystin-2 expression were manifested in the cyst epithelial cells of *Pkd1*$^{-/-}$/LZ^{+} kidneys. Thus, we surmise that polycystin-1 in the primary cilium is required for further inhibition of the proliferation of tubular epithelial cells to maintain their proper size. A *Pkd1*$^{-/-}$ epithelial cell, which is missing negative regulatory signals from polycystin-1, continuously proliferates, and this proliferation induces a "compensatory" proliferation of the surrounding normal epithelial cells in an attempt to re-establish appropriate tubular diameter and structure. This proliferation of tubular epithelial cells accounts for early cyst formation in human ADPKD.

Proliferation of Pkd1$^{-/-}$ *cyst epithelial cells.* EGFR (14, 27), cAMP (28, 29), Wnt/β-catenin (42), and p21 (30) have all been linked to the proliferation of cyst epithelial cells. However, the relationship between activation of these molecules and PKD deficiency is not clear, as those studies assumed that only *PKD*$^{-/-}$ cells proliferated in human ADPKD. Although downregulation of p21 expression in whole embryos of *Pkd1*$^{-/-}$ mice has been suggested to be involved in the proliferation of cyst epithelial cells (30) and we reproduced this downregulation in *Pkd1*$^{-/-}$ kidneys, p21 expression in *Pkd1*$^{-/-}$/LZ^{+} kidneys revealed only a slight decrease. The expression of p53 was significantly decreased in the kidneys of *Pkd1*$^{-/-}$ and *Pkd1*$^{-/-}$/LZ^{+} mice. These results support the findings that p53 expression is decreased in human embryonic kidney 293 cells with loss of polycystin-1 activity (43) and is also slightly decreased in human

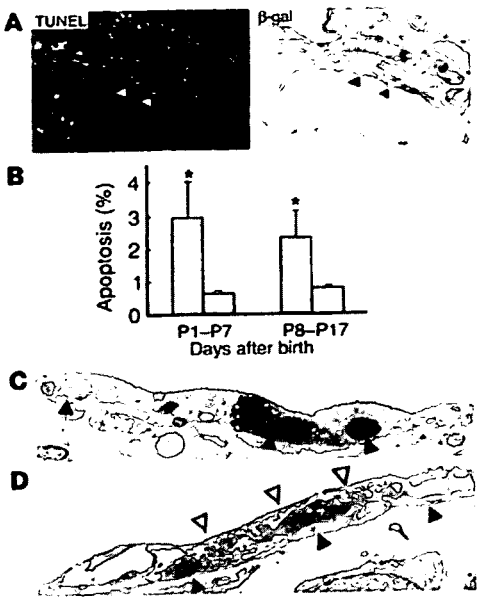

Figure 6
Apoptosis of cyst epithelial cells. (**A**) Apoptosis of cyst epithelial cells in the kidney of a P8 *Pkd1*$^{-/-}$/LZ^{+} mouse was detected by the TUNEL assay. The same section was stained with β-gal and counterstained with Nuclear Fast Red. Arrowheads indicate TUNEL-positive cells. Original magnifications, ×400. (**B**) Summary of results shown in **A**. Each graph represents the percentage of TUNEL-positive cells in LZ^{+} (black bars) and in LZ^{-} (*Pkd1*$^{-/-}$) cyst epithelial cells (white bars), respectively. The mean and SD are from 9 independent mice. *$P < 0.05$. (**C** and **D**) Electron microscopic analysis of the cyst epithelium of a *Pkd1*$^{-/-}$/LZ^{+} kidney. (**C**) Occasional apoptotic cells (black arrowheads) are overlaid by neighboring cells. (**D**) Flat cells (white arrowheads) overlay several degenerated cells that are detached from the tubular basement membrane (black arrowheads). Original magnification, ×1,500.

ADPKD kidneys compared with normal kidneys (26). p53 inhibits cell cycle by induction of p21 (44), and polycystin-1 inhibits Cdk2 activity by upregulation of p21 through the activation of JAK2 (30). Thus, the decrease in p53 in addition to the lack of activation of the JAK-STAT pathway in Pkd1 deficiency may compound the decrease in p21 expression. Because expression of p53, among the cell cycle regulators examined, was affected most strongly in both *Pkd1*$^{-/-}$ cyst epithelial cells and immortalized *Pkd1*$^{-/-}$ MEFs, polycystin-1 may regulate the growth of renal tubular epithelial cells through induction of p53.

Pkd1$^{-/-}$ cyst epithelial cells were not transplantable in nude mice (data not shown). Isolated early cysts from *Pkd1*$^{-/-}$/LZ^{+} kidneys exhibited significant proliferation in vitro with 10% FCS, whereas the proliferation was stunted without FCS (data not shown), suggesting that proliferation of *Pkd1*$^{-/-}$ cyst epithelial cells is not autonomous, as in neoplasms, but instead is growth factor dependent. Among many growth factors and their receptors related with cystogenesis, strong EGFR expression was observed on cystic epithelia of *Pkd1*$^{-/-}$ kidneys (14). Interestingly, EGFR expression increased on both cuboidal and flat cyst epithelial cells in *Pkd1*$^{-/-}$/LZ^{+} kidneys (data not shown). This was supported by the finding of scattered activation of the ERK pathway in both cuboidal and flat cyst epithelial cells in *Pkd1*$^{-/-}$/LZ^{+} kidneys.

Dedifferentiation of Pkd1$^{-/-}$ *cyst epithelial cells.* The cyst epithelia in human ADPKD are composed of cuboidal cells such as normal renal epithelial cells and flat cells (24). A similar phenomenon was noted in *Pkd2*$^{WS25/-}$ kidneys. These 2 morphologically different cells constitute the cyst epithelium at the early and intermediate stages of cystogenesis (45). We also detected 2 kinds of cyst epithelial cells in *Pkd1*$^{-/-}$/LZ^{+} kidneys. Both *Pkd1*$^{-/-}$ and LZ^{+} cyst epithelial cells were cuboidal in shape at the early stage of cystogenesis, and some *Pkd1*$^{-/-}$ cyst epithelial cells changed their shape to flat at the intermediate stage. As LZ^{+} cyst epithelial cells are nearly cuboidal, Pkd1 deficiency is related to the morphological change.

Most flat cyst epithelial cells are negative for nephron segment markers and Na-K ATPase (45), suggesting that the morphological transition of *Pkd1*$^{-/-}$ cyst epithelial cells is accompanied by loss of functional phenotype. However, expression of renal tubular markers within single cysts in *Pkd1*$^{-/-}$/LZ^{+} kidneys was discontinuous. Loss of expression was also detected in the cuboidal cyst epithelial cells at the early stage of cystogenesis. Although there is a tendency for correlation between loss of Na-K ATPase expression and flat shape of cyst epithelial cells, the morphological change of cyst epithelial cells is not completely correlated with the loss of tubular markers.

The cell adhesion molecules E-cadherin and β-catenin are bound to polycystin-1 and polycystin-2 (42), and E-cadherin expression decreases in *Pkd1*$^{-/-}$ kidneys (14). Thus, Pkd1 deficiency may change the polarity of cyst epithelial cells by affecting cell adhesion or

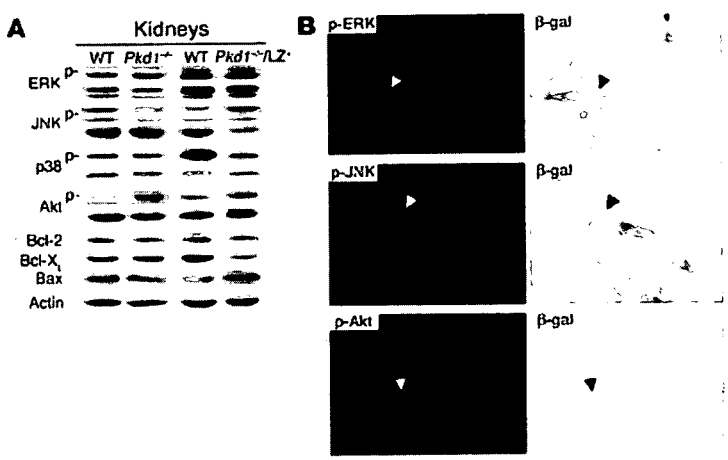

Figure 7
Signaling pathways related to proliferation or apoptosis in cyst epithelial cells. (**A**) Expression of signal transducers in the kidneys of *Pkd1*$^{-/-}$ mice at E16.5 and *Pkd1*$^{-/-}$/LZ^{+} mice 1 month of age was analyzed using Western blot. Actin was used as a loading control for protein. Data presented are 1 representative of 4 independent experiments. (**B**) A kidney from a P8 *Pkd1*$^{-/-}$/LZ^{+} mouse was stained with anti–p-ERK, anti–p-JNK, or anti–p-Akt. The same section was stained with β-gal and counterstained with Nuclear Fast Red. Black and white arrowheads indicate the same epithelial cells. Original magnification, ×400.

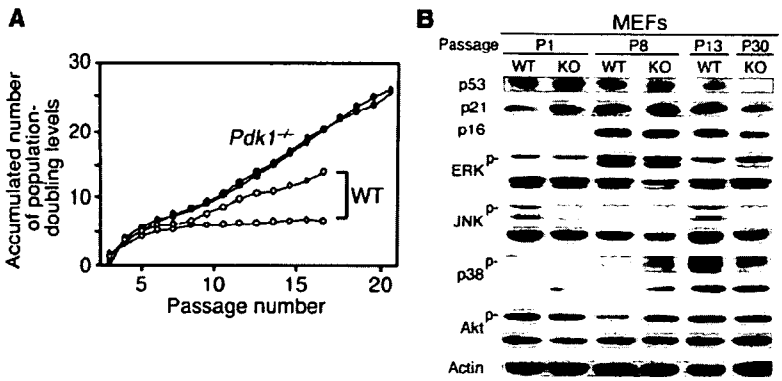

Figure 8
Outgrowing *Pkd1*$^{-/-}$ MEFs. (**A**) The 3T3-type culture of MEFs from *Pkd1*$^{-/-}$ and wild-type mice. (**B**) Signaling pathways related to proliferation or apoptosis in *Pkd1*$^{-/-}$ MEFs. Expression of signal transducers and cell cycle regulators was analyzed using Western blot. Actin was used as a loading control for protein. Data presented are 1 representative of 4 independent experiments.

cytoskeletal organization. However, the localization and intensity of both E-cadherin and β-catenin in some cyst epithelial cells were similar to those in normal renal tubular cells at the intermediate stage of cystogenesis (data not shown). These results indicate that the morphological change in cyst epithelial cells is not due to loss of tubular markers or to repression of cell adhesion molecules. As *Pkd1*$^{-/-}$ cyst epithelial cells cultured in collagen gel sometimes made tubules in the gel (data not shown), outgrowing *Pkd1*$^{-/-}$ cyst epithelial cells retain some functions of renal tubular epithelial cells. Further studies will be done to elucidate the cause of the morphological change and the dedifferentiation (loss of tubular markers) of cyst epithelial cells initiated by deficiency in the *Pkd1* gene.

Apoptosis on normal (LZ^{+}*) cyst epithelial cells.* Apoptosis has been frequently observed in non-dilated and cystic tubuli and glomeruli in ADPKD kidneys, whereas it is extremely rare in normal kidneys (46). In addition, the increased rate of growth in cyst epithelial cells is accompanied by an increased rate of apoptosis in human ADPKD (26). Of note, our study showed that apoptotic cells were present mainly in cuboidal epithelial cells in *Pkd1*$^{-/-}$/LZ^{+} kidneys. Electron microscopy revealed characteristic apoptotic features among cuboidal cyst epithelium, which was covered by flat cells. Apoptotic cells were lost from cyst epithelium and neighboring flat cells lined tubular lumina. These findings suggest net replacement of cuboidal LZ^{+} epithelial cells by flat *Pkd1*$^{-/-}$ epithelial cells.

Expression of p-JNK increased in *Pkd1*$^{-/-}$/LZ^{+} kidneys but not in *Pkd1*$^{-/-}$ kidneys. In contrast, Bcl-X_L expression was decreased in *Pkd1*$^{-/-}$/LZ^{+} kidneys but not in *Pkd1*$^{-/-}$ kidneys. Although p-Akt expression was significantly increased in both cuboidal and flat cyst epithelial cells, cuboidal cyst epithelial cells are more apoptotic than are flat cyst epithelial cells. The 3T3 cell cultures using *Pkd1*$^{-/-}$ MEFs also demonstrated that expression of p-JNK and p-p38 was increased in wild-type MEFs at the cell senescence stage (after passage 13). However, this expression did not increase in immortalized *Pkd1*$^{-/-}$ MEFs until passage 30. As polycystin-1 triggers activation of JNK but not that of p38 (47), flat *Pkd1*$^{-/-}$ epithelial cells and *Pkd1*$^{-/-}$ MEFs in the 3T3 culture escape apoptosis mediated by activation of JNK. These immortalized flat *Pkd1*$^{-/-}$ epithelial cells slowly spread to form large cysts.

A model of cystogenesis. We developed chimeric mice by aggregation of *Pkd1*$^{-/-}$ ES cells and *Pkd1*$^{+/+}$ morulae of LZ^{+} ROSA26 mice. These mice are a unique mouse model for human ADPKD. In *Pkd1*$^{-/-}$/LZ^{+} kidneys, sporadic *Pkd1*$^{-/-}$ epithelial cells deteriorated the entire tubular integrity by the proliferation of both *Pkd1*$^{-/-}$ and normal (LZ^{+}) epithelial cells at the early stage of cystogenesis (Figure 9). When tubular epithelial cells, including *Pkd1*$^{-/-}$ epithelial cells, receive stimulation, both *Pkd1*$^{-/-}$ and normal tubular epithelial cells proliferate to expand the tubular size. The *Pkd1*$^{-/-}$ tubular epithelial cells lack negative signals for proliferation by polycystin-1 and continue to proliferate. Although surrounding normal tubular epithelial cells also proliferate to retain both the round shape and diameter of the tubule, normal epithelial cells are gradually lost by JNK-mediated apoptosis at the intermediate stage. Some *Pkd1*$^{-/-}$ tubular epithelial cells change shape from cuboidal to flat (dedifferentiation), and the flat *Pkd1*$^{-/-}$ epithelial cells grow in an immortalized fashion to form large cysts in the kidney at the late stage of cystogenesis. As p53 expression and JNK activation were very low in flat *Pkd1*$^{-/-}$ cyst epithelial cells, polycystin-1 plays a role in the prevention of immortalized proliferation of renal tubular epithelial cells via p53 induction and JNK activation.

Methods

Generation of Pkd1$^{-/-}$ *mice.* Murine *Pkd1* genomic clones were obtained by screening a 129/Sv mouse genomic library (14). R1 ES cells were transfected with linearized *Pkd1* neomycin-targeting vectors by electroporation and were subjected to positive and negative selection for 14 days using G418 and diphtheria toxin. Approximately 134 clones were examined using Southern blot, and homologous recombination was detected in 18 clones. One independent targeted ES clone was used to generate chimeric mice using the aggregation method (48). DNA from tail tissue of agouti pups

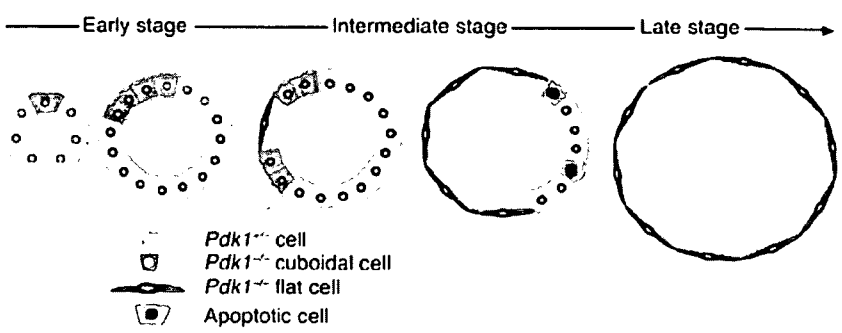

Figure 9
A model schema of the cystogenesis in ADPKD. The germline mutation of 1 allele of the *Pkd1* gene is present in all tubular epithelial cells.

obtained by mating chimeric mice with C57BL/6 mice (Japan SLC) was analyzed using Southern blot. Homozygous mutant pups were generated by intercrossing of heterozygous mutant mice. All procedures conformed to the Chiba University Resolution on Use of Animals in Research and were approved by the Institutional Animal Care and Use Committee of the Graduate School of Medicine, Chiba University (Chiba, Japan).

Generation of Pkd1$^{-/-}$ ES cells and Pkd1$^{-/-}$/LZ^{+} chimeric mice. One of the *Pkd1*-targeted ES clones was transfected by electroporation with linearized *Pkd1* hygromycin targeting vectors to generate *Pkd1*$^{-/-}$ ES cells. Approximately 17 ES clones were examined by Southern blot, and 4 independent *Pkd1*$^{-/-}$ ES clones were obtained. Those *Pkd1*$^{-/-}$ ES cells were aggregated with morulae of ROSA26 mice with the exogenous *LacZ* gene (a gift from H. Koseki, RIKEN Research Center for Allergy and Immunology, Yokohama, Japan) to generate *Pkd1*$^{-/-}$/LZ^{+} chimeric mice.

Southern blot. Genotyping was done by digestion of genomic DNA (10 μg) with *Eco*RV, Southern transfer, and hybridization with a 1.3-kb DNA probe that was external to the targeting vector. The probe was labeled with digoxigenin (Roche Diagnostics) using PCR. The probe detected the wild-type allele as a 15.1-kb fragment and the mutant alleles as 7.7-kb and 8.3-kb fragments.

Histology and immunohistochemistry. Tissues were fixed in 10% phosphate-buffered formalin and were embedded in paraffin. Sections (3 μm thick) were stained with H&E according to standard protocols. For immunohistochemistry, after deparaffinization through a graded xylene and ethanol series, sections were washed in PBS (pH 7.4) and were treated for 15 minutes with 0.3% hydrogen peroxide in methanol. After blocking, sections were stained with the following antibodies: anti-p53, anti-p-EGFR (Santa Cruz Biotechnology Inc.), and anti-PCNA (Sigma-Aldrich). For immunofluorescence, frozen section were stained with YCC2 (anti-polycystin-2; a kind gift from Y. Cai, Yale University, New Haven, Connecticut, USA), anti-β-gal (Chemicon International Inc.), anti-Na-K ATPase (Upstate), anti-acetylated tubulin, anti-DBA, anti-lectin *Lotus tetragonolobus* (Sigma-Aldrich), anti-p-ERK, anti-p-Akt, or anti-p-JNK (Cell signaling Technology Inc.). Photomicrographs were obtained using a microscope (Carl Zeiss International).

β-gal staining of kidneys. Kidneys were fixed for 30 minutes at 4°C in 2.7% formaldehyde, 0.02% NP-40, and 0.2% glutaraldehyde in PBS (pH 7.4) and were washed. Processing was carried out through a graded series of sucrose concentrations from 15% to 30% in PBS at 4°C for 5–12 hours for each step. Kidneys were then embedded in OCT (Tissue-Tek) and were frozen in 2-methyl-butane submerged in liquid nitrogen. Sections (3 μm thick) were then prepared, mounted on slides, and washed in PBS for 5 minutes, and were subsequently stained at 37°C overnight in X-gal solution (1 mg/ml X-gal in DMSO, 2 mM $MgCl_2$, 20 mM potassium ferricyanide, 20 mM potassium ferrocyanide, and 0.02 % NP-40 in PBS). Sections were counterstained with Nuclear Fast Red (Trevigen Inc.).

Microdissection of nephron segments. Nephrons were isolated from the kidneys of wild-type, *Pkd1*$^{-/-}$, and *Pkd1*$^{-/-}$/LZ^{+} mice at E17.5. Microdissection of tubules was done in PBS under a stereomicroscope (2).

Western blot. Kidneys were sonicated in Tris lysis buffer (20 mM Tris-HCl, 150 mM NaCl, 100 mM NaF, 1 mM EDTA, 1 mM sodium orthovanadate, 1 mM phenylmethylsulfonyl fluoride, 1.5 nM aprotinin, and 10 nM leupeptin). Proteins were separated by SDS-PAGE and were transferred to polyvinylidene difluoride membranes (Millipore). Membranes were blocked with nonfat dry milk (Yukijirushi) and were incubated with the following antibodies: anti-p53, anti-p21, anti-ERK, anti-Bcl-X_L, anti-Bax, anti-p16, anti-actin (Santa Cruz Biotechnology Inc.), anti-Akt, anti-p-Akt, anti-p-ERK, anti-p38, anti-p-p38 (Cell Signaling Technology Inc.), anti-JNK, anti-p-JNK (BD Biosciences-Pharmingen), or anti-Bcl-2 (R&D Systems). The filters were washed with TBS/0.1% Triton-X, and immunoreactive bands were visualized by enhanced chemiluminescence.

In vitro culture of microdissected tubules. Microdissection of tubules was done in L-15 medium (Sigma-Aldrich) followed by culture at 37°C in 5% CO_2 in collagen gel (Neutral Solution, DMEM Culture Medium; Koken) in DMEM supplemented with 10% FCS (Sigma-Aldrich).

TUNEL assay. Animals were perfused with a solution of 4% paraformaldehyde in 0.1 M phosphate buffer (pH 7.4). Organs were dissected and were post-fixed overnight with 4% paraformaldehyde. The tissues were equilibrated with 20% sucrose and were cut into sections 3 μm in thickness on a cryostat. The TUNEL assay was carried as described with slight modification (49). The tailing reaction was carried out for 1 hour at 37°C in TdT buffer in the presence of dUTP-biotin (The Mebstain Apoptosis kit, Medical & Biological Laboratories). Signals were visualized using Avidin-Rohdamine (Vector Laboratories). Sections were counterstained with DAPI (Molecular Probes).

Electron microscopy. Specimens were fixed in formalin followed by 2% glutaraldehyde, were post-fixed with 1% osmium tetroxide, and were embedded in epoxy resin mixture. Ultrathin sections were mounted on grids, stained with uranyl acetate-lead citrate, and observed under a transmission electron microscope (Hitachi).

Cell culture. MEFs were established from *Pkd1*$^{-/-}$ embryos (E13.5). Heads and livers were removed from embryos, and the remaining embryonic tissues were trypsinized at 37°C for 30 minutes. The disrupted tissues were plated in DMEM supplemented with 10% FCS (Sigma-Aldrich) and were cultured at 37°C in 5% CO_2. The 3T3-type serial MEF cultivation was done as described (38). Briefly, 3×10^5 cells were plated on a 6-cm well; 3 days later, the total number of cells was counted, and 3×10^5 cells were plated on a separate well. The cumulative increase in cell number was calculated according to the formula $\mathrm{Log}(N_f / N_i)/\mathrm{Log}2$, where N_i is the initial number of cells plated and N_f is the final number of cells counted after 3 days.

Statistical analysis. Data presented represents the mean ± SD of more than 3 independent experiments. Statistical analysis was performed using an unpaired Student's *t* test. *P* values of less than 0.05 were considered to be significant.

Acknowledgments

We are grateful to H. Koseki and S. Somlo for discussions and to Y. Cai for providing YCC2 (anti-polycystin-2). We also thank L. Fujimura, H. Satake, K. Hanaoka, J. Usui, S. Horita, and H. Hazawa for skillful technical assistance; N. Kakinuma for secretarial services; and M. Ohara for language assistance. This work was supported in part by Grants-in-Aid from the Ministry of Education, Science, Technology, Sports and Culture of Japan, a grant from the Inamori Foundation (to T. Mochizuki), and a grant from Sankyo Foundation of Life Science (to T. Mochizuki).

Received for publication July 28, 2004, and accepted in revised form January 11, 2005.

Address correspondence to: Toshio Mochizuki, Department of Medicine II, Hokkaido University Graduate School of Medicine, Kita 15, Nishi 7, Kita-ku, Sapporo 060-8638, Japan. Phone: 81-11-716-1161; Fax: 81-11-706-7710; E-mail: mtoshi@med.hokudai.ac.jp.

1. Gabow, P.A. 1993. Autosomal dominant polycystic kidney disease. *N. Engl. J. Med.* **329**:332–342.
2. Baert, L. 1978. Hereditary polycystic kidney disease (adult form): a microdissection study of two cases at an early stage of the disease. *Kidney Int.* **13**:519–525.
3. Wilson, P.D. 2004. Polycystic kidney disease. *N. Engl. J. Med.* **350**:151–164.
4. The European Polycystic Kidney Disease Consortium. 1994. The polycystic kidney disease 1 gene encodes a 14 kb transcript and lies within a duplicated region on chromosome 16. The

European Polycystic Kidney Disease Consortium. *Cell.* **77**:881–894.
5. Mochizuki, T., et al. 1996. PKD2, a gene for polycystic kidney disease that encodes an integral membrane protein. *Science.* **272**:1339–1342.
6. Watnick, T.J., et al. 1998. Somatic mutation in individual liver cysts supports a two-hit model of cystogenesis in autosomal dominant polycystic kidney disease. *Mol. Cell.* **2**:247–251.
7. Qian, F., Watnick, T.J., Onuchic, L.F., and Germino, G.G. 1996. The molecular basis of focal cyst formation in human autosomal dominant polycystic kidney disease type I. *Cell.* **87**:979–987.
8. Pei, Y., et al. 1999. Somatic PKD2 mutations in individual kidney and liver cysts support a "two-hit" model of cystogenesis in type 2 autosomal dominant polycystic kidney disease. *J. Am. Soc. Nephrol.* **10**:1524–1529.
9. Brasier, J.L., and Henske, E.P. 1997. Loss of the polycystic kidney disease (PKD1) region of chromosome 16p13 in renal cyst cells supports a loss-of-function model for cyst pathogenesis. *J. Clin. Invest.* **99**:194–199.
10. Torra, R., et al. 1999. A loss-of-function model for cystogenesis in human autosomal dominant polycystic kidney disease type 2. *Am. J. Hum. Genet.* **65**:345–352.
11. Lu, W., et al. 1999. Late onset of renal and hepatic cysts in Pkd1-targeted heterozygotes. *Nat. Genet.* **21**:160–161.
12. Wu, G., et al. 1998. Somatic inactivation of Pkd2 results in polycystic kidney disease. *Cell.* **93**:177–188.
13. Lu, W., et al. 1997. Perinatal lethality with kidney and pancreas defects in mice with a targetted Pkd1 mutation. *Nat. Genet.* **17**:179–181.
14. Muto, S., et al. 2002. Pioglitazone improves the phenotype and molecular defects of a targeted Pkd1 mutant. *Hum. Mol. Genet.* **11**:1731–1742.
15. Boulter, C., et al. 2001. Cardiovascular, skeletal, and renal defects in mice with a targeted disruption of the Pkd1 gene. *Proc. Natl. Acad. Sci. U. S. A.* **98**:12174–12179.
16. Lu, W., et al. 2001. Comparison of Pkd1-targeted mutants reveals that loss of polycystin-1 causes cystogenesis and bone defects. *Hum. Mol. Genet.* **10**:2385–2396.
17. Sutters, M., and Germino, G.G. 2003. Autosomal dominant polycystic kidney disease: molecular genetics and pathophysiology. *J. Lab. Clin. Med.* **141**:91–101.
18. Igarashi, P., and Somlo, S. 2002. Genetics and pathogenesis of polycystic kidney disease. *J. Am. Soc. Nephrol.* **13**:2384–2398.
19. Nauli, S.M., et al. 2003. Polycystins 1 and 2 mediate mechanosensation in the primary cilium of kidney cells. *Nat. Genet.* **33**:129–137.
20. Yoder, B.K., Hou, X., and Guay-Woodford, L.M. 2002. The polycystic kidney disease proteins, polycystin-1, polycystin-2, polaris, and cystin, are co-localized in renal cilia. *J. Am. Soc. Nephrol.* **13**:2508–2516.
21. Lin, F., et al. 2003. Kidney-specific inactivation of the KIF3A subunit of kinesin-II inhibits renal ciliogenesis and produces polycystic kidney disease. *Proc. Natl. Acad. Sci. U. S. A.* **100**:5286–5291.
22. McGrath, J., Somlo, S., Makova, S., Tian, X., and Brueckner, M. 2003. Two populations of node monocilia initiate left-right asymmetry in the mouse. *Cell.* **114**:61–73.
23. Lubarsky, B., and Krasnow, M.A. 2003. Tube morphogenesis: making and shaping biological tubes. *Cell.* **112**:19–28.
24. Grantham, J.J., Geiser, J.L., and Evan, A.P. 1987. Cyst formation and growth in autosomal dominant polycystic kidney disease. *Kidney Int.* **31**:1145–1152.
25. Nadasdy, T., et al. 1995. Proliferative activity of cyst epithelium in human renal cystic diseases. *J. Am. Soc. Nephrol.* **5**:1462–1468.
26. Lanoix, J., D'Agati, V., Szabolcs, M., and Trudel, M. 1996. Dysregulation of cellular proliferation and apoptosis mediates human autosomal dominant polycystic kidney disease (ADPKD). *Oncogene.* **13**:1153–1160.
27. Wilson, P.D., Du, J., and Norman, J.T. 1993. Autocrine, endocrine and paracrine regulation of growth abnormalities in autosomal dominant polycystic kidney disease. *Eur. J. Cell Biol.* **61**:131–138.
28. Yamaguchi, T., et al. 2003. Cyclic AMP activates B-Raf and ERK in cyst epithelial cells from autosomal-dominant polycystic kidneys. *Kidney Int.* **63**:1983–1994.
29. Hanaoka, K., and Guggino, W.B. 2000. cAMP regulates cell proliferation and cyst formation in autosomal polycystic kidney disease cells. *J. Am. Soc. Nephrol.* **11**:1179–1187.
30. Bhunia, A.K., et al. 2002. PKD1 induces p21(waf1) and regulation of the cell cycle via direct activation of the JAK-STAT signaling pathway in a process requiring PKD2. *Cell.* **109**:157–168.
31. Ong, A.C., et al. 1999. Polycystin-1 expression in PKD1, early-onset PKD1, and TSC2/PKD1 cystic tissue. *Kidney Int.* **56**:1324–1333.
32. Ward, C.J., et al. 1996. Polycystin, the polycystic kidney disease 1 protein, is expressed by epithelial cells in fetal, adult, and polycystic kidney. *Proc. Natl. Acad. Sci. U. S. A.* **93**:1524–1528.
33. Geng, L., et al. 1996. Identification and localization of polycystin, the PKD1 gene product. *J. Clin. Invest.* **98**:2674–2682.
34. Griffin, M.D., Torres, V.E., Grande, J.P., and Kumar, R. 1996. Immunolocalization of polycystin in human tissues and cultured cells. *Proc. Assoc. Am. Physicians.* **108**:185–197.
35. Weston, B.S., et al. 1997. Polycystin expression during embryonic development of human kidney in adult tissues and ADPKD tissue. *Histochem. J.* **29**:847–856.
36. Nauta, J., Goedbloed, M.A., van den Ouweland, A.M., Nellist, M., and Hoogeveen, A.T. 2000. Immunological detection of polycystin-1 in human kidney. *Histochem. Cell Biol.* **113**:303–311.
37. Zambrowicz, B.P., et al. 1997. Disruption of overlapping transcripts in the ROSA beta geo 26 gene trap strain leads to widespread expression of beta-galactosidase in mouse embryos and hematopoietic cells. *Proc. Natl. Acad. Sci. U. S. A.* **94**:3789–3794.
38. Todaro, G.J., and Green, H. 1963. Quantitative studies of the growth of mouse embryo cells in culture and their development into established lines. *J. Cell Biol.* **17**:299–313.
39. Kamijo, T., et al. 1997. Tumor suppression at the mouse INK4a locus mediated by the alternative reading frame product p19ARF. *Cell.* **91**:649–659.
40. Loghman-Adham, M., Nauli, S.M., Soto, C.E., Kariuki, B., and Zhou, J. 2003. Immortalized epithelial cells from human autosomal dominant polycystic kidney cysts. *Am. J. Physiol. Renal Physiol.* **285**:F397–F412.
41. Bernstein, J., and Gilbert-Barness, E. 1994. Congenital malformation of the kidney. In *Renal pathology.* B. Brenner, editor. J.B. Lippincott Co. Philadelphia, Pennsylvania, USA. 1366 pp.
42. Huan, Y., and van Adelsberg, J. 1999. Polycystin-1, the PKD1 gene product, is in a complex containing E-cadherin and the catenins. *J. Clin. Invest.* **104**:1459–1468.
43. Kim, H., Bae, Y., Jeong, W., Ahn, C., and Kang, S. 2004. Depletion of PKD1 by an antisense oligodeoxynucleotide induces premature G1/S-phase transition. *Eur. J. Hum. Genet.* **12**:433–440.
44. Gartel, A.L., and Tyner, A.L. 1999. Transcriptional regulation of the p21((WAF1/CIP1)) gene. *Exp. Cell Res.* **246**:280–289.
45. Thomson, R.B., et al. 2003. Histopathological analysis of renal cystic epithelia in the Pkd2WS25/- mouse model of ADPKD. *Am. J. Physiol. Renal Physiol.* **285**:F870–F880.
46. Woo, D. 1995. Apoptosis and loss of renal tissue in polycystic kidney diseases. *N. Engl. J. Med.* **333**:18–25.
47. Arnould, T., et al. 1998. The polycystic kidney disease 1 gene product mediates protein kinase C alpha-dependent and c-Jun N-terminal kinase-dependent activation of the transcription factor AP-1. *J. Biol. Chem.* **273**:6013–6018.
48. Wood, S.A., Allen, N.D., Rossant, J., Auerbach, A., and Nagy, A. 1993. Non-injection methods for the production of embryonic stem cell-embryo chimaeras. *Nature.* **365**:87–89.
49. Kojima, S., et al. 2001. Testicular germ cell apoptosis in Bcl6-deficient mice. *Development.* **128**:57–65.

nature genetics

A functional variant in *FCRL3*, encoding Fc receptor-like 3, is associated with rheumatoid arthritis and several autoimmunities

Yuta Kochi[1,2], Ryo Yamada[1], Akari Suzuki[1], John B Harley[3], Senji Shirasawa[4], Tetsuji Sawada[2], Sang-Cheol Bae[5], Shinya Tokuhiro[1], Xiaotian Chang[1], Akihiro Sekine[6], Atsushi Takahashi[7], Tatsuhiko Tsunoda[7], Yozo Ohnishi[8], Kenneth M Kaufman[3], Changsoo Paul Kang[9], Changwon Kang[9], Shigeru Otsubo[10], Wako Yumura[11], Akio Mimori[4], Takao Koike[12], Yusuke Nakamura[10,13], Takehiko Sasazuki[4] & Kazuhiko Yamamoto[1,2]

Rheumatoid arthritis is a common autoimmune disease with a complex genetic etiology. Here we identify a SNP in the promoter region of *FCRL3*, a member of the Fc receptor-like family, that is associated with susceptibility to rheumatoid arthritis (odds ratio = 2.15, $P = 0.00000085$). This polymorphism alters the binding affinity of nuclear factor-κB and regulates *FCRL3* expression. We observed high *FCRL3* expression on B cells and augmented autoantibody production in individuals with the disease-susceptible genotype. We also found associations between the SNP and susceptibility to autoimmune thyroid disease and systemic lupus erythematosus. *FCRL3* may therefore have a pivotal role in autoimmunity.

Rheumatoid arthritis is one of the most common autoimmune diseases and is characterized by inflammation of synovial tissue and joint destruction. Although the disease is believed to result from a combination of genetic and environmental factors, its complete etiology has not yet been clarified[1]. Specific haplotypes of human leukocyte antigen (HLA)-DRB1, usually referred to as shared-epitope sequences[2], have been repeatedly reported to confer susceptibility to rheumatoid arthritis[3,4]; other genetic components are also involved[5]. This combination of HLA haplotypes and non-HLA genes accounting for disease susceptibility is also observed for other autoimmune diseases[6–8]. In autoimmune thyroid disease (AITD), for instance, the *HLA-DR3* haplotype is associated with disease risk, as is a functional haplotype of a non-HLA gene, *CTLA4*, that has recently been associated with AITD susceptibility[9].

Identification of non-HLA genes associated with rheumatoid arthritis susceptibility and other autoimmunities seems difficult, because of the low relative risk of disease resulting from these non-HLA genes compared with the strong relative risk from disease-associated HLA haplotypes. In a search for non-HLA determinants of disease susceptibility, whole-genome studies have been done for both human autoimmune diseases and experimental animal models. These studies have identified nonrandom clustering of susceptibility loci for clinically distinct diseases[8,10]. The overlap of susceptibility loci for multiple autoimmunities suggests that common susceptibility genes exist in those regions. Intense studies of loci-clustering regions identified genes commonly associated with multiple autoimmune diseases, such as *CTLA4* on 2q33 (ref. 9), *SLC22A4* and *SLC22A5* on 5q31 (ref. 11) and *PTPN22* on 1p13 (ref. 12).

Cytoband 1q21–23 is one of the regions implicated in susceptibility to multiple autoimmune diseases. The Fcγ receptor (FcγR) II/III genes are located at 1q23, and a new family of genes, Fc receptor-like genes (FCRLs, also known as FcRHs[13,14], IRTAs[15,16] or SPAPs[17]), clusters nearby at 1q21 (**Fig. 1a**). FCRLs have high structural homology with classical FcγRs, although their ligands and function are not yet known. These receptors are good candidates for involvement in autoimmunity, as they are believed to be involved in the pathogenesis of rheumatoid arthritis and other autoimmune diseases[18]. Region 1q23 is a candidate locus for susceptibility to systemic lupus erythematosus

[1]Laboratory for Rheumatic Diseases, SNP Research Center, RIKEN, Yokohama 230-0045, Japan. [2]Department of Allergy and Rheumatology, Graduate School of Medicine, the University of Tokyo, Tokyo 113-0033, Japan. [3]University of Oklahoma; US Department of Veterans Affairs; and Oklahoma Medical Research Foundation, Oklahoma City, Oklahoma 73104, USA. [4]International Medical Center of Japan, Tokyo 162-8655, Japan. [5]Department of Internal Medicine, Division of Rheumatology, the Hospital for Rheumatic Diseases, Hanyang University, Seoul 133-792, Republic of Korea. Laboratories for [6]Genotyping, [7]Medical Informatics and [8]SNP Analysis, SNP Research Center, RIKEN, Yokohama 230-0045, Japan. [9]Department of Biological Sciences, Korea Advanced Institute of Science and Technology, Daejeon 305-701, Republic of Korea. [10]Laboratory of Molecular Medicine, Human Genome Center, Institute of Medical Science, the University of Tokyo, Tokyo 108-8639, Japan. [11]Department of Medicine, Kidney Center, Tokyo Women's Medical University, Tokyo 162-8666, Japan. [12]Department of Medicine II, Hokkaido University School of Medicine, Sapporo 060-8638, Japan. [13]Research Group for Personalized Medicine, SNP Research Center, RIKEN, Yokohama 230-0045, Japan. Correspondence should be addressed to R.Y. (ryamada@src.riken.go.jp).

Published online 17 April 2005; doi:10.1038/ng1540

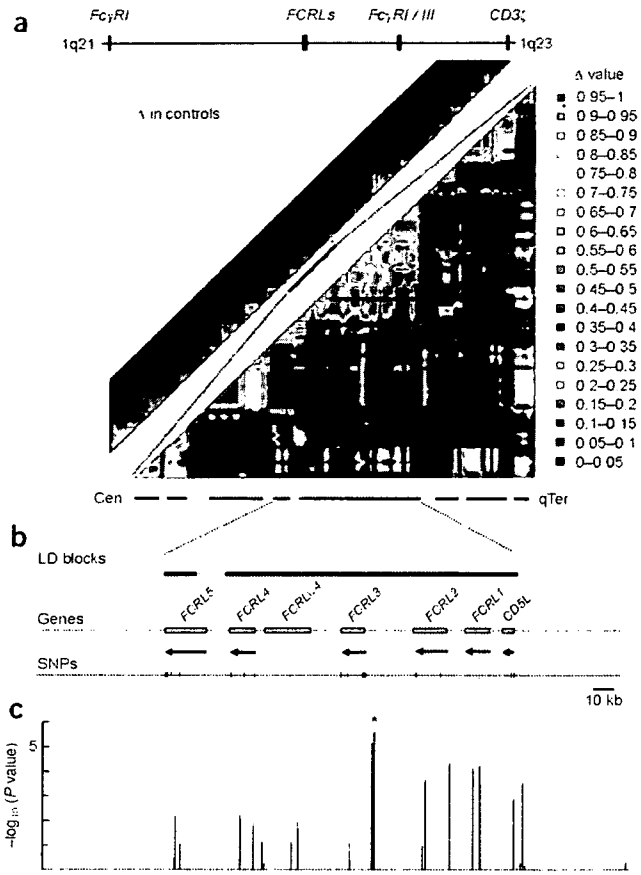

Figure 1 LD and association of the FCRL gene cluster. (a) Pairwise LD between SNPs, as measured by Δ in 658 controls. The 16-Mb region in 1q21–23 (upper left) and the 2-Mb region around the FCRL gene cluster (lower right) were evaluated. (b) Location of LD blocks, genes and 41 SNPs in the FCRL gene cluster. (c) Case-control association test with 41 SNPs in the FCRL gene cluster using 830 affected individuals and 658 controls. *Peak association.

(SLE), and variants in the classical FcγR II/III genes partially account for disease susceptibility[6,19]. Region 1q21 is a candidate locus for susceptibility to psoriasis (*PSORS4*; refs. 7,20) and multiple sclerosis[21]. The mouse homologous region to human 1q21, on chromosome 3, also contains susceptibility loci for multiple autoimmune disease models[8], including collagen-induced arthritis (*Cia5*, also called *Mcia2* (ref. 22); *Eae3* (ref. 23); *Tmevd2* (ref. 24); *Idd10*; and *Idd17* (ref. 25)). Although 1q21–23 is a good candidate region for containing rheumatoid arthritis–susceptibility genes, the association of classical FcγRs with disease susceptibility remains controversial[26,27]. Here we focused on the 1q21–23 region to identify rheumatoid arthritis–associated genes in Japanese subjects using linkage disequilibrium (LD) mapping.

RESULTS

Case-control study by SNP-based LD mapping at 1q21–23

To evaluate the extent of association, we analyzed LD with SNPs distributed in a 16-Mb region on 1q21–23, including the FCRL gene cluster and the classical FcγRs (**Fig. 1a**). We genotyped 658 control subjects for 742 SNPs from the JSNP database and selected 491 SNPs with allele frequency >0.1, successful genotyping rate >0.95 and $P >$ 0.01 with Hardy-Weinberg equilibrium testing for evaluation of LD. We calculated the pairwise LD index Δ (ref. 28) for each pair of SNPs, identifying 110 LD blocks[11] at a threshold of $\Delta > 0.5$ (**Fig. 1a**).

For association testing, we examined the Japanese set of 830 cases and 658 controls used for LD block evaluation. We initially genotyped 94 rheumatoid arthritis cases for 491 SNPs and compared their allele frequencies with those of 658 control subjects. We identified nine SNPs that had allele frequencies differing by more than 0.1 between 658 controls and 94 cases with $P < 0.01$. We genotyped the remaining cases for these nine SNPs and tested their allele frequencies for case-control association. We identified the smallest P value between an intronic SNP in the gene *FCRL3* and rheumatoid arthritis (fcrl3_6, $P = 1.8 \times 10^{-5}$; association was statistically significant in both rheumatoid arthritis subgroups (94 and 736 individuals)). This SNP was located in a LD block containing four of the five FCRL genes; the fifth was in the adjacent block. We therefore evaluated the origin of this association in these two LD blocks (**Fig. 1b**), although our results do not exclude the presence of variants associated with rheumatoid arthritis or other autoimmune diseases in other LD blocks at 1q21–23.

In addition to the 25 SNPs of the 491 that we used for LD block evaluation, we identified 16 additional SNPs in exons and 5′ and 3′ flanking regions of five FCRL genes and one pseudogene (*FCRLψ4*) by searching the public database and sequencing genomic DNA from Japanese individuals with rheumatoid arthritis. We genotyped these 16 SNPs in the identical case and control samples (830 cases, 658 controls) to increase the density of variants in the targeted region. We observed a peak of association in a short segment consisting of four SNPs in *FCRL3* ($P < 1.0 \times 10^{-4}$; **Fig. 1c** and **Supplementary Table 1** online): fcrl3_3, fcrl3_4, fcrl3_5 and fcrl3_6, located at nt −169, −110, +358 (5′ untranslated region of exon 2) and +1381 (intron 3; 204 bp and 859 bp from the 3′ and 5′ ends of the flanking exons) relative to the transcription initiation site, respectively.

We observed the smallest P value without correction in recessive-trait genotype comparison of fcrl3_3 in *FCRL3* ($P = 8.5 \times 10^{-7}$; odds ratio = 2.15; 95% confidence interval = 1.58–2.93; **Table 1**). This

Table 1 Case-control analysis of *FCRL3*

			Allele 1 frequency		Genotype 11 versus 12 + 22		
SNP	Location	Allele (1/2)	Affected individuals	Controls	OR (95% c.i.)	χ^2	P
fcrl3_3	−169	C/T	0.42	0.35	2.15 (1.58–2.93)	24.3	0.00000085
fcrl3_4	−110	A/G	0.25	0.18	3.01 (1.71–5.29)	16.1	0.000060
fcrl3_5	Exon 2	C/G	0.42	0.35	2.05 (1.51–2.78)	21.6	0.0000033
fcrl3_6	Intron 3	A/G	0.42	0.34	2.02 (1.49–2.75)	20.8	0.0000052

SNPs with $P < 0.0001$ in allele frequency comparison test are shown. c.i., confidence interval; OR, odds ratio.

Table 2 Haplotype structure and frequency in *FCRL3*

Haplotype	Sequence (fcrl3_3-4-5-6)	Frequency: Affected individuals	Frequency: Controls
1	TGGG	0.58	0.65
2	CACA	0.25	0.19
3	CGCA	0.17	0.14

Haplotypes with frequency >0.01 are shown.

P value was still significant when the most conservative Bonferroni correction was applied (comparisons for 507 SNPs; corrected $P = 0.00043$). The four strongly associated SNPs were in LD with each other, and we inferred three common haplotypes (**Table 2**); fcrl3_3, fcrl3_5 and fcrl3_6 showed strong LD with each other ($\Delta > 0.99$), whereas fcrl3_4 showed relatively weak LD with the other three SNPs (mean $\Delta = 0.68$).

To identify causal variants in this segment on the basis of genotype data, we carried out a forward stepwise-regression procedure with a cut-off *P* value to proceed to the next step of 0.01 (ref. 29). No SNP in FCRL genes other than *FCRL3* improved the model. None of the four SNPs in *FCRL3* were preferred over the others in these data (data not shown). This result implied that one of the SNPs in *FCRL3* might cause the disease, but the possibility remained that variants in other genes were truly associated with the disease.

To validate the case-control association test, we evaluated the impact of population stratification on the case-control study (830 cases, 658 controls). We selected 2,069 SNPs, each of which was identified as a tagging SNP[30] in 2,069 distinct LD segments that were previously identified by genotyping 74,842 SNPs distributed in autosomal chromosomes[31]. We analyzed population structure[32] and the χ^2 sum[33] to evaluate stratification but detected no significant evidence of population stratification (**Supplementary Fig. 1** online). These results are suggestive of no or negligible stratification of our samples and support the validity of the case-control association results by removing this confounding factor from further consideration.

Regulatory effect of SNP −169C→T on *FCRL3* expression

Because none of the four SNPs in *FCRL3* (fcrl3_3, fcrl3_4, fcrl3_5 and fcrl3_6) produces amino-acid substitutions, we assessed potential effects of the SNPs on transcription factor binding using TRANSFAC software. Nuclear factor-κB (NF-κB) was predicted to bind the sequence containing the rheumatoid arthritis–susceptibility allele fcrl3_3 (−169C) with a high score (core match 1.000, matrix match 0.957); substitution with the nonsusceptible allele T decreased the score of NF-κB binding substantially (core match 0.760, matrix match 0.824). The other three SNPs were not predicted to bind to any transcriptional factor with high score, and nucleotide substitution was not predicted to affect binding at any regulatory factor. We therefore focused on the 5′ flanking region of fcrl3_3 to explore the regulatory effects on expression of *FCRL3*.

We carried out reporter gene analysis using the genomic sequence of *FCRL3* from nt −523 to +203. We made constructs corresponding to the three haplotypes using SNPs at nt −169 (C→T, fcrl3_3) and −110 (G→A, fcrl3_4; **Fig. 2a**) and used them to transfect Raji cells, a Burkitt's lymphoma cell line that expresses *FCRL3* (ref. 13) and is derived from germinal center B cells. Luciferase activity was substantially greater in cells transfected with −169C −110G or −169C −110A constructs than in cells transfected with −169T −110G constructs. This suggests that SNP −169C→T is crucial for regulation of *FCRL3* expression. To clarify, we cloned single or four tandem copies of 30-bp

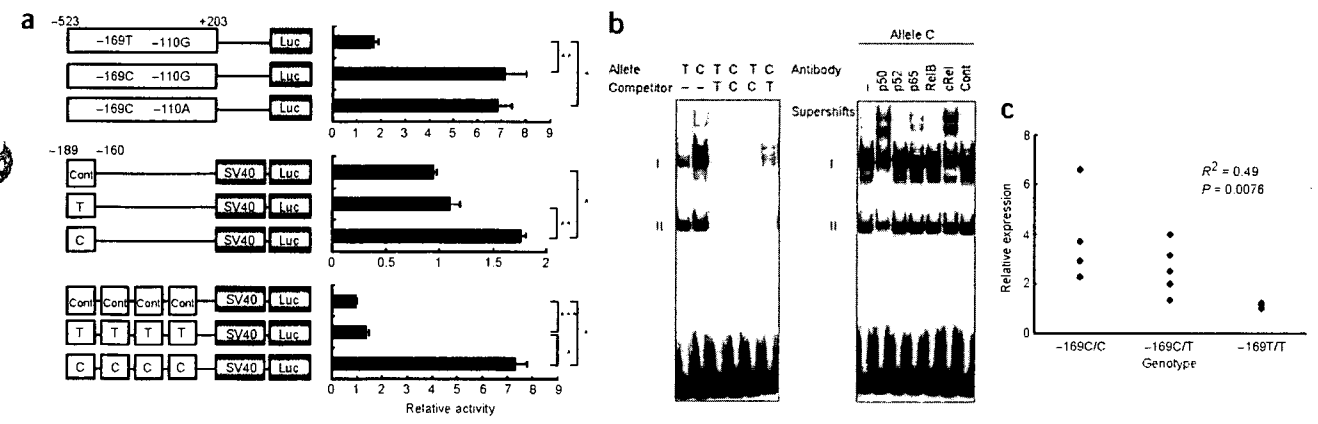

Figure 2 Correlation of *FCRL3* expression with allele and genotype. (**a**) Promoter activity of haplotypes in *FCRL3* (top) and enhancing activity of the 30-bp promoter region around −169C→T (middle and bottom), as evaluated by luciferase assay. Data represent mean ± s.e.m. Representative data from three experiments done in quadruplicate. $^*P < 0.0001$; $^{**}P < 0.001$; $^{***}P < 0.01$ by Student's *t*-test. (**b**) Binding affinity of nuclear factors to the 30-bp promoter region around −169C→T evaluated by EMSA. Allelic difference and competition experiment (left) and supershift experiment using antibodies for NF-κB components (right). (**c**) Expression of *FCRL3* measured by quantitative TaqMan PCR of RNA purified from $CD19^+$ B cells obtained from 13 healthy volunteers (C/C, $n = 4$; C/T, $n = 5$; T/T, $n = 4$). (**d**) ASTQ. *FCRL3* transcripts in B cells and genomic DNA from individuals ($n = 5$) with heterozygous genotypes (−169C/T +358C/G) were amplified and quantified using an *EagI* restriction-fragment length polymorphism located at position +358. The 122-bp and 85-bp bands represent transcripts of the +358C allele and +358G allele, respectively. Transcripts from homozygous individuals (+358C/C and +358G/G) are shown as controls for digestion.

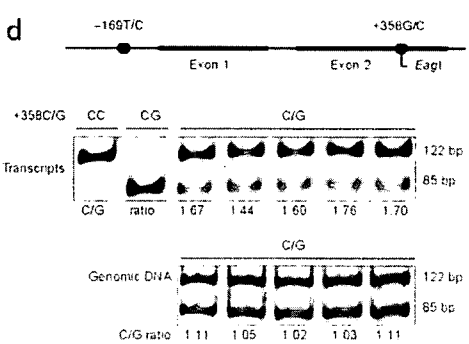

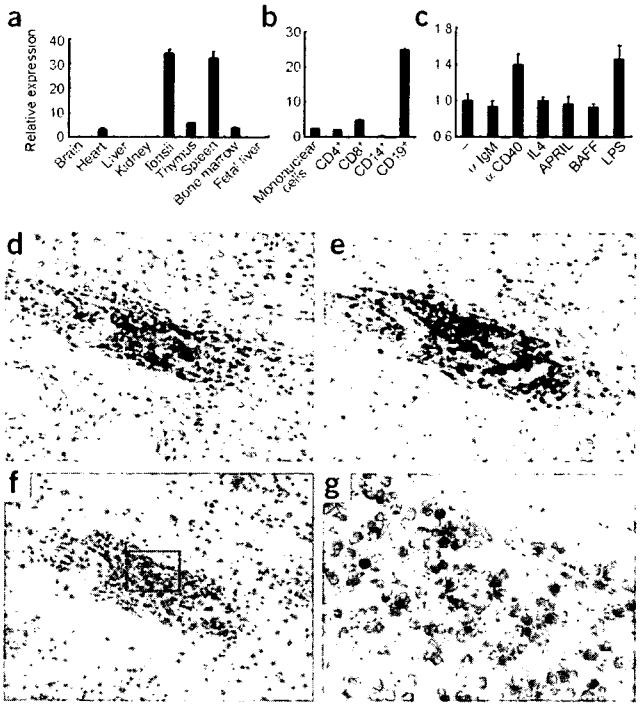

Figure 3 Expression patterns of *FCRL3* in human tissues and cells. (**a**) Relative expression of *FCRL3* in various tissues. (**b**) Relative expression of *FCRL3* in fractionated leukocytes using MTC panel (Clontech). (**c**) Relative expression of *FCRL3* in response to stimuli (antibody to CD40, 1 μg ml^{-1}; antibody to IgM, 1 μg ml^{-1}; IL-4, 10 ng ml^{-1}; APRIL, 10 ng ml^{-1}; BAFF, 10 ng ml^{-1}; LPS, 100 ng ml^{-1}) for 4 h. Representative data from three experiments done in triplicate. (**d**,**e**) Lymphocyte aggregates in rheumatoid arthritis synovium. T cells and B cells in serial sections were immunostained using antibodies to CD3 (**d**) and CD20 (**e**), respectively. (**f**,**g**) *FCRL3* mRNA expression (blue stain) in rheumatoid arthritis synovium as analyzed by *in situ* hybridization. Higher magnification views of synovium (**g**) are denoted by the box in **f** (magnifications: **d**–**f**, ×100; **g**, ×400). Counterstaining: **d**,**e**, hematoxylin; **f**,**g**, nuclear fast red.

oligonucleotides surrounding SNP −169C→T and control oligonucleotides into a vector with the SV40 promoter. Cells transfected with a single copy of the C allele produced substantially greater luciferase activity than cells transfected with a single copy of the T allele. More convincingly, transfection with four tandem copies of the C allele enhanced luciferase activity by a factor of 20 over transfection with four tandem copies of the T allele (**Fig. 2a**).

To elucidate specific nuclear factors that bind the disease-susceptible allele, we analyzed the sequence around −169C→T. These sequences were predicted by TRANSFAC software to have binding affinity for NF-κB, which regulates a wide variety of genes in the immune system. The disease-susceptible sequence (including −169C) had higher matrix similarity to the consensus NF-κB binding motif than the nonsusceptible sequence (including −169T). We then carried out electrophoretic mobility shift assays (EMSAs) to examine whether differences between the susceptible −169C allele and the nonsusceptible −169T allele affected binding of nuclear proteins from Raji cells. We used the same 30-bp labeled oligonucleotides used in the luciferase assay. These sequences contain the predicted NF-κB binding site. We observed two main bands, I and II, in the presence of nuclear extracts; the intensity of band I was higher for the susceptible −169C allele than for the nonsusceptible −169T allele (**Fig. 2b**). Competition assays with unlabeled oligonucleotides indicated that these complexes were specific for the probes. In addition, competition assays with unlabeled probes of the C allele for T and the T allele for C showed that the C allele was better able to compete for binding, a result consistent with the higher binding affinity of labeled C allele probes alone. We also carried out a supershift experiment with antibodies specific for NF-κB components (p50, p52, p65, RelB and cRel). We observed supershifts in some lanes with specific antibodies for p50, p65 and cRel (**Fig. 2b**). Among these, only antibody to p50 shifted band II, suggestive of the presence of a p50-p50 homodimer. Band I had the highest intensity and a substantial allelic difference and was supershifted by antibodies to p50, p65 and cRel. Although these findings indicate that band I comprises a mixture of heterodimers, the greater shifts caused by antibodies to p50 and cRel suggest that the main component is a p50-cRel heterodimer.

The two *in vitro* assays showed the potent transcriptional activity of the disease-susceptible haplotype regulated by NF-κB, suggesting that expression of *FCRL3* is greater from the disease-susceptible −169C allele than from the nonsusceptible −169T allele. To extend these findings, we quantified expression of *FCRL3* in peripheral blood B cells from healthy donors using quantitative TaqMan methods and analyzed the effect of the number of susceptible copies on the transcript level by regression model. Regression analysis identified a significant positive correlation between number of susceptible chromosomes and transcription level ($R^2 = 0.49$, $P = 0.0076$; **Fig. 2c**).

We also carried out allele-specific transcript quantification[9,34] to confirm the effect of the SNP on transcription. Using an *EagI* restriction-fragment length polymorphism located at position +358 in exon 2 of *FCRL3* (fcrl3_5, +358C→G), we measured the relative contribution of each haplotype to transcript production in heterozygous individuals (**Fig. 2d**). We evaluated the transcripts of five doubly heterozygous individuals with genotype −169C/T +358C/G; the mean ratio (susceptible versus nonsusceptible haplotype) was 1.63, significantly higher than that of DNA amplicons (ratio = 1.06, $P < 1 \times 10^{-5}$) from the same individuals. (The quantity of template DNA from the two haplotypes was equal.) These results show that the

Table 3 Genotype and autoantibodies in individuals with rheumatoid arthritis

	RF		Antibody to CCP	
Genotype	*n*[a]	Serum level[b] (IU/ml)	*n*[c]	Positivity (%)
−169C/C	29	479.9 ± 91.3[d]	17	100.0[e]
−169C/T	75	323.7 ± 47.3[d]	35	94.3[e]
−169T/T	44	216.4 ± 44.0[d]	19	73.7[e]

[a]$N = 148$. [b]Mean ± s.e.m. [c]$N = 71$. [d]$R^2 = 0.049$, $P = 0.0065$ by regression analysis. [e]$P = 0.029$ by Fisher's exact test.

Table 4 Association of SNP −169C→T with AITD and SLE

		Genotype				Recessive-trait comparison		
Disease	*n*	CC	CT	TT	Allele C frequency	OR (95% c.i.)	χ^2	*P*
GD	351	72	179	100	0.46	1.79 (1.34–2.39)	15.7	0.000074
HT	158	30	74	54	0.42	1.62 (1.07–2.47)	5.2	0.022
AITD total	509	102	253	154	0.45	1.74 (1.35–2.24)	18.5	0.000017
SLE	564	100	259	205	0.41	1.49 (1.16–1.92)	9.8	0.0017
RA* + AITD + SLE	2,437	438	1,167	832	0.42	1.52 (1.29–1.79)	24.2	0.00000084
Control	2,037	257	995	785	0.37			

*Rheumatoid arthritis represents sum of three sets (n = 1,364). c.i., confidence interval; GD, Graves' disease; HT, Hashimoto's thyroiditis; OR, odds ratio; RA, rheumatoid arthritis.

expression of *FCRL3* is higher in individuals with the disease-susceptible haplotype and suggest that higher expression of *FCRL3* is a potential cause and component of the pathological mechanism(s) leading to rheumatoid arthritis.

Expression of *FCRL3* mRNA

We then quantified *FCRL3* expression in multiple tissues using TaqMan methods. Expression of *FCRL3* transcripts was high in the spleen and tonsils (**Fig. 3a**), which are secondary lymphoid organs. We observed lower expression in thymus and bone marrow. In human blood fractions, $CD19^+$ cells, which represent the B-cell population, had the greatest *FCRL3* expression among peripheral blood mononuclear cells. $CD4^+$ and $CD8^+$ cells had less expression (**Fig. 3b**). We next examined the effect of B-cell stimulation on *FCRL3* expression. We cultured peripheral blood B cells from a healthy donor for 4 h using known B-cell stimulants and then quantified *FCRL3* mRNA (**Fig. 3c**). Expression of *FCRL3* was increased by antibody to CD40 and lipopolysaccharide (LPS).

We then investigated expression of *FCRL3* transcripts in synovial tissue using *in situ* hybridization methods. T and B cells are the key players with regard to inflammation in synovial tissue, producing proinflammatory cytokines and autoantibodies that might be pathogenic[1]. These cells show three distinct histological patterns: diffuse infiltration, clustering in aggregates and follicles with germinal-center reaction[35,36]. We observed aggregations of T and B cells in paraffin-embedded synovial sections from individuals with rheumatoid arthritis, using immunostaining with antibodies to CD3 and CD20, respectively (**Fig. 3d,e**). *In situ* hybridization assay with serial sections detected *FCRL3* mRNA in aggregated lymphocytes (**Fig. 3f,g**). Although strict differentiation between B and T cells was difficult, at least some aggregated B cells were positive, with strong expression of *FCRL3* mRNA. Synovium from two other individuals with rheumatoid arthritis had similar lymphocyte aggregates and *FCRL3* expression (**Supplementary Fig. 2** online).

SNP association with autoantibody and *HLA-DRB1* status

Because we suspected that higher *FCRL3* expression led to B-cell abnormalities in rheumatoid arthritis, we examined associations in individuals with rheumatoid arthritis between genotype and two rheumatoid arthritis–related autoantibodies: rheumatoid factor (RF) and antibody to cyclic citrullinated peptide (CCP). RF is a well-known autoantibody for the Fc region of IgG, and titers correlate with rheumatoid arthritis disease activity[37]. Antibody to CCP recognizes peptides containing citrulline and is detected in rheumatoid arthritis with extremely high specificity[38,39]. RF titer in individuals with rheumatoid arthritis was significantly positively correlated with the number of susceptible alleles (R^2 = 0.049, P = 0.0065; **Table 3**). The positive ratio of antibody to CCP in individuals with rheumatoid arthritis also differed significantly among genotypes ($P < 0.05$) and correlated with number of susceptible alleles.

Because genetic interactions between HLA and non-HLA loci have been described in susceptibility for rheumatoid arthritis and other autoimmune diseases[26,40], we compared genotype distributions for SNP −169C→T among three rheumatoid arthritis subgroups stratified by number of *HLA-DRB1* shared-epitope alleles. We previously genotyped *HLA-DRB1* in our population and observed significant associations between rheumatoid arthritis susceptibility and shared-epitope alleles[4]. Allele frequency of the rheumatoid arthritis–susceptibility allele −169C was significantly higher in the subgroup with two copies of shared-epitope alleles (0.49, n = 113) than in the subgroup with no shared-epitope alleles (0.39, n = 215; $P < 0.05$).

Replication study of association in three autoimmunities

To confirm associations between the *FCRL3* variant and rheumatoid arthritis susceptibility, we carried out a replication study (540 individuals with rheumatoid arthritis, 636 controls). We compared allele frequency and found a significant association between fcrl3_3 (−169C→T) and rheumatoid arthritis susceptibility (allele frequency was 0.40 in individuals with rheumatoid arthritis versus 0.46 in controls; P = 0.041; **Supplementary Table 2** online). We noted no significant differences between two cohorts that consisted of the replication samples. These results further confirmed the association of the fcrl3_3 −169C allele with rheumatoid arthritis susceptibility in Japanese individuals.

Because this region is associated with multiple autoimmune diseases, and because several variants are involved in multiple autoimmunities, we investigated associations between SNP −169C→T and two other autoimmune diseases: AITD and SLE. We recruited 509 Japanese individuals with AITD (351 with Graves' disease and 158 with Hashimoto's thyroiditis) and 564 Japanese individuals with SLE and compared them with 2,037 Japanese controls. In addition, we combined AITD, SLE and rheumatoid arthritis cases as subjects with an autoimmune phenotype and tested for associations with the SNP. Individual diseases, as well as combination of two AITDs and combination of AITD, SLE and rheumatoid arthritis, were significantly associated with the SNP (odds ratio = 1.52, P = 0.00000084 in Japanese for a recessive model between all four autoimmunities considered in aggregate and controls; **Table 4**). As rheumatoid arthritis–specific autoantibodies were correlated with the number of susceptible alleles, antibody to DNA titer was higher in individuals with SLE with genotype −169C/C than in subjects with other genotypes (294.1 IU ml^{-1} versus 145.5 IU ml^{-1}; n = 120; P = 0.026 by Student's t-test), a conclusion not further established by regression analysis (P = 0.12).